


The RING-finger ubiquitin E3 ligase TaPIR1 targets TaHRP1 for degradation to suppress chloroplast function

Received: 2 January 2024

Accepted: 31 July 2024

Published online: 12 August 2024

 Check for updates

Rongrong Zhang^{1,2,4}, Yu Wu^{1,2,4}, Xiangru Qu^{1,2}, Wenjuan Yang^{1,2}, Qin Wu^{1,2}, Lin Huang^{1,2}, Qiantao Jiang^{1,2}, Jian Ma^{1,2}, Yazhou Zhang^{1,2}, Pengfei Qi^{1,2}, Guoyue Chen^{1,2}, Yunfeng Jiang^{1,2}, Youliang Zheng^{1,2}, Xiaojie Wang³✉, Yuming Wei^{1,2}✉ & Qiang Xu^{1,2}✉

Chloroplasts are key players in photosynthesis and immunity against microbial pathogens. However, the precise and timely regulatory mechanisms governing the control of photosynthesis-associated nuclear genes (PhANGs) expression in plant immunity remain largely unknown. Here we report that TaPIR1, a *Pst*-induced RING-finger E3 ubiquitin ligase, negatively regulates *Pst* resistance by specifically interacting with TaHRP1, an atypical transcription factor histidine-rich protein. TaPIR1 ubiquitinates the lysine residues K¹³¹ and K¹³⁶ in TaHRP1 to regulate its stability. TaHRP1 directly binds to the TaHRP1-binding site elements within the PhANGs promoter to activate their transcription via the histidine-rich domain of TaHRP1. PhANGs expression induces the production of chloroplast-derived ROS. Although knocking out *TaHRP1* reduces *Pst* resistance, *TaHRP1* overexpression contributes to photosynthesis, and chloroplast-derived ROS production, and improves disease resistance. *TaPIR1* expression inhibits the downstream activation of TaHRP1 and TaHRP1-induced ROS accumulation in chloroplasts. Overall, we show that the TaPIR1-mediated ubiquitination and degradation of TaHRP1 alters PhANGs expression to disrupt chloroplast function, thereby increasing plant susceptibility to *Pst*.

Plants are continuously exposed to several potential pathogens. In response, they have evolved a refined, two-branched defense system to protect themselves against such disease-causing agents^{1–3}. The first layer of defense involves multiple plasma membrane-localized pattern recognition receptors that can detect pathogen-associated molecular patterns (PAMPs) such as chitin and flagellin (Flg22), which elicit various immune responses, including callose deposition, reactive oxygen species (ROS) accumulation, and defense-related gene expression⁴. To achieve successful invasion, pathogens deliver various effectors into host cells to suppress their basal immune

response by interfering with host immune factors, such as receptors and downstream signaling factors. In addition, plants employ specific disease resistance genes (R genes) to detect pathogen-secreted effectors. The strong interaction between effectors and R proteins remarkably induces disease resistance that rivals the specificity and range of the mammalian adaptive immune system⁵. Notably, the production of immune signals such as ROS and nitric oxide (NO) induces salicylic acid (SA) synthesis at infection sites. Increased SA levels further elicit plant defense responses in a self-amplifying feedback loop, ultimately leading to a hypersensitive response (HR)–

¹State Key Laboratory of Crop Gene Exploration and Utilization in Southwest China, Sichuan Agricultural University, Chengdu, China. ²Triticeae Research Institute, Sichuan Agricultural University, Chengdu, China. ³State Key Laboratory for Crop Stress Resistance and High-Efficiency Production, College of Plant Protection, Northwest A&F University, Yangling, China. ⁴These authors contributed equally: Rongrong Zhang, Yu Wu. ✉ e-mail: wangxiaojie@nwsuaf.edu.cn; ymwei@sicau.edu.cn; xuqiang1264700418@163.com

a type of cell necrosis that occurs at infection sites to restrict pathogen spread^{6,7}.

In plants, chloroplasts play key roles in immunity as major sites for the production of carbohydrates and the generation of various defense signals, such as SA, Ca²⁺, and NO signals. In chloroplasts, isochorismate synthase catalyzes the conversion of chorismate into isochorismate, which is further converted into SA^{8,9}. A chloroplast-localized protein, calcium-sensing receptor (CAS), plays a role in the formation of chloroplast-derived Ca²⁺ transients and regulates SA biosynthesis to control plant innate immunity¹⁰. SA acts as a key regulator not only in PAMPs-triggered immunity and effectors-triggered immunity (ETI) but also in systemic acquired resistance, which refers to broad-spectrum and systemic resistance to secondary infections. Importantly, when plant tissues encounter biotic or abiotic stress, chloroplasts can reprogram and integrate secondary metabolite synthesis, phytohormone crosstalk, and communication with other organelles via retrograde signaling^{11,12}. In addition, chloroplasts are crucial contributors to redox homeostasis, including ROS generation. The ROS in chloroplasts includes hydroxyl radicals (OH•), hydrogen peroxide (H₂O₂), and singlet-excited oxygen (¹O₂)¹³. Excess light absorption to the maximum capacity of the photosynthetic electron transport chain (PETC) for CO₂ assimilation induces the production of ¹O₂ and H₂O₂ from photosystem I (PSI) and PSII¹⁴. Excessive ROS accumulation limits pathogen colonization at infection sites. Moreover, ROS serves as retrograde signaling molecules that induce nuclear gene expression. Several studies have provided insights into chloroplast-mediated plant immunity against microbial pathogens. In *Arabidopsis*, the reduction of PsbS, a subunit of photosystem II, contributed to energy dissipation by protecting the photosystems from damage caused by excess light and enhanced photosynthesis-induced ROS accumulation after the perception of PAMP¹⁵. In wheat, the chloroplast-targeted kinase WKS1 encoded by the rust resistance gene *Yr36* interacts with and phosphorylates PsbO, a PSII oxygen-evolving enhancer protein 1, to disrupt the photosystem and confer resistance to *Pst*¹⁶. The stable silencing of *TaSP*, which encodes a subunit of the Cyt b6/f complex, inhibits photosynthesis and chloroplast-derived ROS accumulation, resulting in the reduced resistance of plants to avirulent *Pst*¹⁷. Although numerous studies on chloroplast function have reported the role of chloroplast-targeting proteins in plant immunity, the precise and timely regulatory mechanisms of transcription in controlling the expression of chloroplast-associated nuclear genes in wheat remain largely unknown.

Ubiquitination, an essential post-translational regulatory process, involves the enzymatic attachment of a chain of ubiquitin molecules to target proteins. This modification via a mega-complex protease, 26S proteasome, marks the target proteins for degradation^{18,19}. Ubiquitination is achieved through the sequential activities of the ubiquitin-activating enzyme E1, ubiquitin-conjugating enzyme E2, and ubiquitin ligase E3²⁰. In plants, ubiquitination E3 ligases can be subdivided into three classes, namely, U-box, homologous to E6-associated protein C-terminus, and really interesting new gene (RING)-type E3 ligases²¹. Several studies have reported the role of ubiquitination in various cellular processes, including hormone responses, development, and immunity. In rice, microtubule-associated E3 ligase ubiquitinates serine hydroxymethyltransferase and promotes its degradation to induce broad-spectrum resistance²². In addition, two E3 ubiquitin ligases, RIP1 and APIP6, fine-tuned the Ca²⁺ sensor ROD1 to inhibit ROS scavenging by reducing the catalase activity of CatB, ultimately conferring resistance to multiple pathogens^{23,24}. By contrast, the rice scaffold protein OsCUL3a of the E3 ubiquitin ligase complex interacts with and degrades OsNPR1 via 26S proteasome, thus negatively affecting cell death and plant immunity²⁵. However, compared with the ubiquitination processes in rice, the role of ubiquitin ligase E3 in wheat immunity and its mode of substrate recognition remains unclear.

Herein, we identified a RING-finger ubiquitin E3 ligase, *TaPIR1*, as a susceptibility factor that plays a negative role in inducing *Pst* resistance in wheat. The *TaPIR1* knockout in hexaploid wheat induced broad-spectrum resistance to the *Pst* races CYR31 and CYR34. *TaPIR1* physically interacted with and ubiquitinated an atypical transcription factor histidine-rich protein, *TaHRP1*, which directly regulates photosynthesis-associated nuclear genes (PhANGs) expression. Although the loss of *TaHRP1* drastically reduced *Pst* resistance in wheat, its overexpression contributed to chloroplast-derived ROS accumulation and improvement in disease resistance. The *TaPIR1*-induced binding and modification of *TaHRP1* to suppress PhANGs expression may affect the production of chloroplast-derived ROS, as well as photosynthesis. Overall, these findings indicate that *TaPIR1*-mediated ubiquitination and degradation of *TaHRP1* act as a switch to disrupt chloroplast function and ROS accumulation, increasing plant susceptibility to *Pst*.

Results

TaPIR1 is a negative defense regulator against *Pst* in wheat

Among the differentially expressed genes in *Pst*-infected wheat leaves²⁶, the expression of *TaPIR1-4A* (*Puccinia striiformis*-induced RING-finger protein 1), a member of the E3 ubiquitin-protein ligase family, was induced at 24 h post-inoculation (hpi), as described in the quantitative reverse transcription polymerase chain reaction (qRT-PCR) results (Supplementary Fig. 1a). Despite 99% nucleotide sequence similarity among the three copies of *TaPIR1* located on chromosomes 4AS, 4BS, and 4DS, the *TaPIR1-4A* and *TaPIR1-4B* transcripts exhibited significant induction incompatible interactions, approximately by threefold, at 24 hpi; however, the *TaPIR1-4D* transcripts remained undetected (Supplementary Fig. 1a). To understand the role of *TaPIR1* in wheat-*Pst* interaction, we first employed barley stripe mosaic virus (BSMV)-induced gene silencing to knock down *TaPIR1* expression. At 10 days after BSMV inoculation, photobleaching was observed in *Phytoene desaturase* (*TaPDS*)-silenced plants, which served as a positive control. Compared with the control plants, the *TaPIR1*-silenced wheat plants exhibited fewer urediniospore pustules and a typical HR when wheat plants expressing the BSMV constructs were infected with *Pst* CYR34 at 14 days post-infection (dpi) (Supplementary Fig. 1b). The *TaPIR1* transcript exhibited a 60–70% reduction at 24 hpi and 48 hpi in plants expressing the BSMV construct of *TaPIR1* (Supplementary Fig. 1c). The *TaPIR1*-silenced plants exhibited lower *Pst* biomass than the control plants (Supplementary Fig. 1d). Furthermore, we overexpressed *TaPIR1* in Fielder plants and inoculated with *Pst* CYR23. Compared with the control plants, the *TaPIR1*-expressing plants exhibited urediniospore pustules (Supplementary Fig. 1e). Consistently, the *TaPIR1*-overexpressing plants showed a >60–70% increase in fungal biomass compared with that of the controls (Supplementary Fig. 1f), indicating a negative role in wheat stripe rust resistance.

To further validate the role of *TaPIR1* in inducing plant susceptibility to *Pst*, the three *TaPIR1* homologs (*TaPIR1-4A*, *TaPIR1-4B*, and *TaPIR1-4D*) in the wheat cultivar Fielder were edited via CRISPR-Cas9 gene editing. However, only two mutant plants, which contained nucleotide deletions leading to frameshift mutations in the region targeted by Cas9 in *TaPIR1-4A* and *TaPIR1-4B* (*tapir1-AB*) or *TaPIR1-4A* alone (*tapir1-A*), were obtained using three pairs of primers specific to the abovementioned three *TaPIR1* homologs (Supplementary Fig. 2a). When inoculated with the predominant *Pst* races CYR31 and CYR34, the T₂ generation of *tapir1-AB* and *tapir1-A* plants exhibited a strong HR and contained a few urediniospore pustules (Fig. 1a and Supplementary Fig. 2b). Notably, compared with the wild-type (WT) plants, *tapir1-AB* and *tapir1-A* plants exhibited 50–60% reductions in fungal biomass (Fig. 1b and Supplementary Fig. 2c). The stable knockout of *tapir1-AB* also reduced the hyphal length and infection areas of *Pst* CYR34 at 24 hpi and 48 hpi (Fig. 1c, d). The *tapir1-AB* plants demonstrated

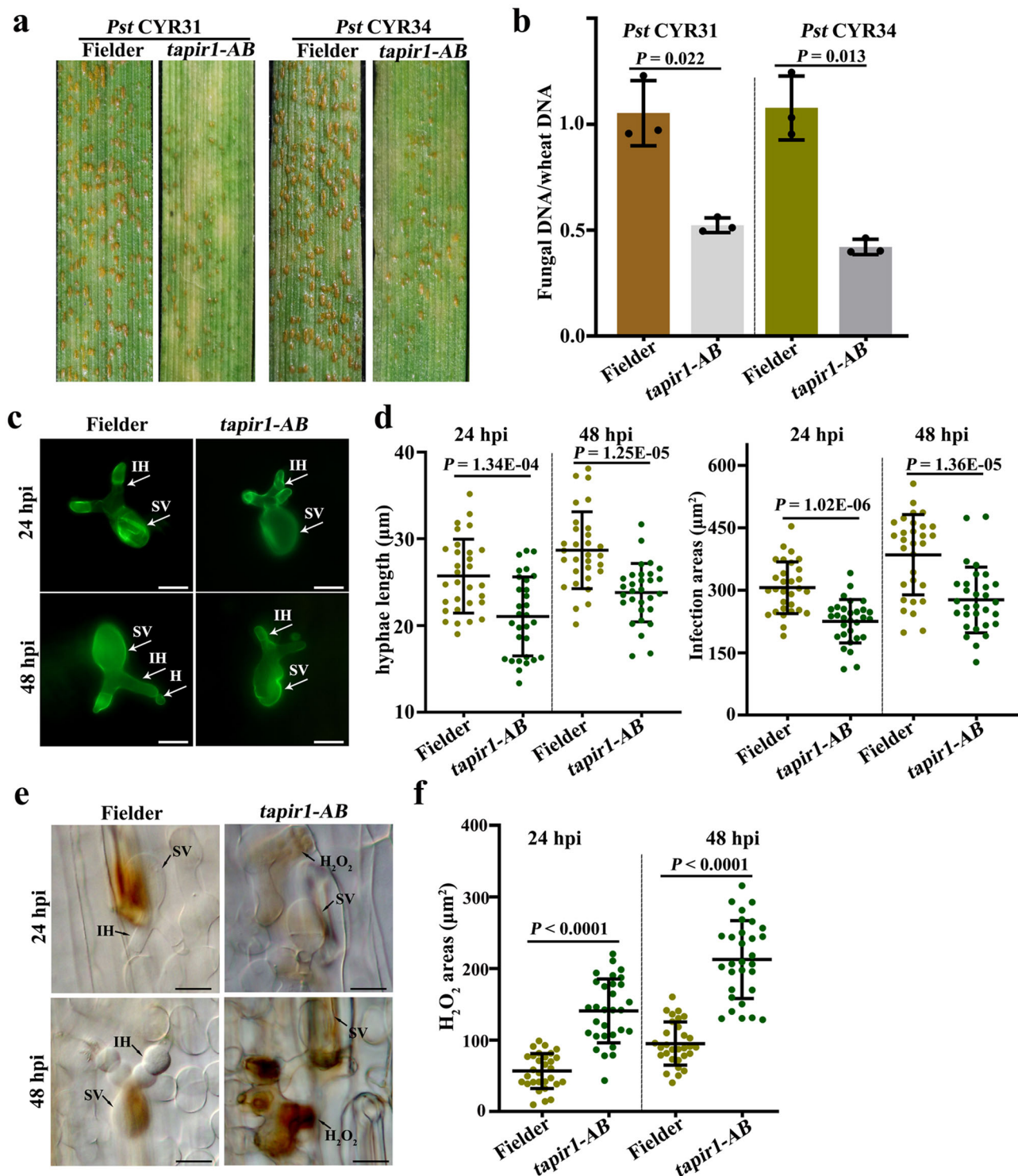


Fig. 1 | TaPIR1 negatively regulates wheat resistance to *Pst*. The second leaves of the seedlings of the *TaPIR1* knockout plant (*tapir1-AB*) and Fielder were infected with *Pst* CYR31 and CYR34, respectively. **a** *Pst* uredinia on the second leaves of *tapir1-AB* and Fielder were observed at 14 dpi. **b** The *Pst*/wheat biomass ratio was measured at 120 hpi via qRT-PCR of DNA isolated from the same set of wheat plants, as shown in (a). The internal control genes *TaEF* and *PstEF* were used to normalize the DNA levels of wheat and *Pst*, respectively. Values are mean \pm standard deviation (SD), $n = 3$ biologically independent samples. The P value was determined by a two-tailed unpaired Student's t -test. **c** Representative images were obtained from *tapir1-AB* and Fielder plants inoculated with *Pst* CYR34 at 24 hpi or 48 hpi using CellSens Entry software. IH infectious hyphae, SV substomatal vesicle, bar = 20 μm . **d** Hyphal

length and infection areas on the same set of wheat plants, as shown in (c), were evaluated using CellSens Entry software. Means \pm SD were calculated from 30 infection sites of three independent biological repeats. The P value was determined by a two-tailed unpaired Student's t -test. **e** Histological analysis of H_2O_2 accumulation in *tapir1-AB* and Fielder plants inoculated with *Pst* CYR34 at 24 hpi and 48 hpi. SV substomatal vesicle, IH infectious hyphae, bar = 20 μm . **f** H_2O_2 accumulation in the same wheat samples was assessed at 24 hpi and 48 hpi using CellSens Entry software as described above. Means \pm SD were calculated from 30 infection sites of three independent biological repeats. The P value was determined by a two-tailed unpaired Student's t -test. Source data are provided as a Source Data file.

markedly greater ROS accumulation than Fielder plants at 24 hpi and 48 hpi (Fig. 1e, f). These results indicate that TaPIR1 negatively regulates *Pst* resistance in wheat.

TaPIR1 interacts with and ubiquitinates TaHRP1

To verify the predicted nuclear localization sequence (NLS) in the C-terminal region, the TaPIR1:green fluorescent protein (GFP) construct driven by the CaMV35s promoter was first generated for transient infiltration in *Nicotiana benthamiana*. GFP signals were specifically observed in the nucleus of the resulting tobacco cells expressing TaPIR1:GFP, whereas control-free GFP was distributed throughout the cells (Supplementary Fig. 3a). Repeated experiments in wheat protoplasts revealed the specific nuclear localization of the green fluorescence of TaPIR1:GFP upon transient transfection of the TaPIR1:GFP construct (Supplementary Fig. 3b).

To further explore the molecular mechanism by which TaPIR1 influences the plant immune response, we used TaPIR1-4B as a bait to screen the yeast two-hybrid (Y2H) library of *Pst*-infected wheat leaves for TaPIR1-interacting proteins. In total, 45 clones were identified as 32 plant proteins (Supplementary Data 1). Owing to the nucleus localization of TaPIR1, we focused on nucleoproteins. Among the 32 interactants, all 13 nucleus-related interactants were identified and used to detect interactions with TaPIR1. Only TaHRP1, heavy metal-associated isoprenylated protein (TaHMAI), and histone H1 (TaH1) were confirmed to interact with TaPIR1 by the Y2H system. The yeast cells expressing pBD:TaPIR1-pAD:TaHRP1, pBD:TaPIR1-pAD:TaH1, and pBD:TaPIR1-pAD:TaHMAI grew on SD-Ade plates and exhibited galactosidase activity (Fig. 2a and Supplementary Data 1).

To further analyze the physical interaction between TaPIR1 and its interactants, they were fused with the C- and N-terminal portions of yellow fluorescent protein (YFP), respectively, using the bimolecular fluorescence complementation (BiFC) assay. The fused products were transformed into *Agrobacterium tumefaciens* and then infiltrated into tobacco leaves. The fluorescence signals of the TaPIR1-TaHRP1 interaction were specifically observed in the nucleus (Fig. 2b). By contrast, fluorescence signals remained undetected when TaPIR1:cYFP-TaH1:nYFP and TaPIR1:cYFP-TaHMAI:nYFP were transiently expressed (Fig. 2b). Furthermore, the *in vitro* pull-down assay indicated that glutathione S-transferase (GST):TaHRP1 can effectively pull down TaPIR1:His compared with the GST control, suggesting a physical interaction between TaPIR1 and TaHRP1 (Fig. 2c). In addition, we performed the coimmunoprecipitation (Co-IP) assay in tobacco leaves cotransformed with TaPIR1:GFP/TaHRP1:HA, as well as the total protein extracted from tobacco leaves and mixed with GFP-trap beads. HRP1:HA was coimmunoprecipitated by TaPIR1:GFP but not by GFP alone, indicating that TaPIR1 interacts with TaHRP1 *in vivo* (Fig. 2d). To identify the TaHRP1-interacting region, we artificially truncated the disordered region in TaPIR1 predicted via DISOPRED 3 and generated bait constructs of TaPIR1 mutants (Supplementary Fig. 4a). However, all TaPIR1-truncated mutants failed to interact with TaHRP1 in yeast (Supplementary Fig. 4b). Furthermore, TaPIR1 interacted with TdHRP1 derived from *Triticum durum* but not with HvHRP1 derived from *Hordeum vulgare*, although their protein sequences were 80% identical to the TaHRP1 sequence (Supplementary Fig. 4c–e). Overall, these findings confirm that TaPIR1 physically interacts with TaHRP1 in the nucleus.

To analyze E3 ligase activity in TaPIR1, we first expressed and purified His-tagged TaPIR1:His derived from *Escherichia coli* (Supplementary Fig. 3c) and performed an *in vitro* ubiquitination assay. When TaPIR1:His was incubated with purified E1, E2, and ubiquitin, a protein ladder of polyubiquitinated TaPIR1:His was detected using anti-ubiquitin antibodies, indicating that TaPIR1 possesses E3 ligase activity and can mediate self-ubiquitination *in vitro* (Supplementary Fig. 3d). However, TaPIRIM, in which His-60 and His-235 were replaced

by alanine in the RING structure, lost E3 ligase activity *in vivo* (Supplementary Fig. 3e). We further analyzed whether TaHRP1 can be used as a ubiquitination substrate for TaPIR1. In the presence of TaPIR1:His, E1, E2, and TaHRP1:GST, a strong protein ladder of polyubiquitinated TaHRP1:GST was detected (Fig. 2e). However, in the absence of E1, E2, TaPIR1:His (E3) or TaHRP1, no TaHRP1 polyubiquitination was observed (Fig. 2e). To further determine whether TaPIR1 contributes to TaHRP1 ubiquitination *in vivo*, immunoprecipitation assay was performed. As expected, more ubiquitinated TaHRP1 proteins were detected in the protoplasts prepared from *TaPIR1OE* or *tapir1-AB*-expressing *TaPIR1* compared with Fielder plants; however, ubiquitinated TaHRP1 proteins rarely appeared in the protoplasts prepared from *tapir1-AB* (Fig. 2f). Consistent with this result, an *in vivo* ubiquitination assay revealed that TaHRP1 is ubiquitinated in *N. benthamiana* co-expressing *TaPIR1*. However, TaPIRIM was not observed to ubiquitinate TaHRP1 in *N. benthamiana* (Supplementary Fig. 5a). Collectively, these results demonstrate that TaPIR1 is a functional E3 Ub ligase that can ubiquitinate the TaHRP1 protein.

TaPIR1 promotes TaHRP1 degradation

Considering that TaPIR1 directly interacts with TaHRP1 and ubiquitinates it both *in vitro* and *in vivo*, we determined whether the E3 ligase TaPIR1 affects TaHRP1 protein turnover. TaHRP1 stability was evaluated based on cell-free degradation analysis of the total protein extracts derived from the loss-of-function mutants *tapir1-AB*, Fielder plants, and *TaPIR1*-overexpressing plants. Compared with GST control, TaHRP1:GST accelerated degradation in coinubation mixtures from Fielder plants but were relatively stable in coinubation mixtures from *tapir1-AB* compared with Fielder plants extracts (Fig. 3a and Supplementary Fig. 5b). In contrast to the Fielder plants extracts, incubation with extracts from *TaPIR1*-overexpressing plants significantly increased the degradation rate of TaHRP1:GST (Fig. 3a). In all coinubation mixtures, the presence of MG132 inhibited TaHRP1:GST degradation (Fig. 3a). In addition, TaHRP1:GFP exhibited a lower amount of protein in *TaHRP1*-overexpressing plants infected with *Pst* CYR34 compared with that in uninfected plants (Supplementary Fig. 2g). In addition, more TaHRP1 proteins were detected in the protoplasts prepared from *tapir1-AB* compared with Fielder plants; however, the TaHRP1 protein abundance was reduced in the protoplasts prepared from *tapir1-AB*-expressing *TaPIR1* or *TaPIR1OE* plants (Supplementary Fig. 3f). Consistent with this result, an *in vivo* degradation assay revealed that TaPIR1 promoted TaHRP1 degradation in wheat protoplasts co-expressing *TaPIR1* but TaPIRIM could not (Supplementary Fig. 5c). We obtained similar results in *N. benthamiana*, wherein TaHRP1 protein levels were affected by TaPIR1, but TaPIRIM did not have the same effect (Fig. 3b). Based on these results, we concluded that TaPIR1 ubiquitinates TaHRP1, leading to its degradation by the 26S proteasome.

TaHRP1 degradation depends on its lysine residues K¹³¹ and K¹³⁶

We further analyzed the potential ubiquitination sites of TaHRP1 and found that six lysine residues were present in the C-terminal region of TaHRP1. K¹³¹ and K¹³⁶ residues of TaHRP1 protein were predicted as the most likely ubiquitination sites (Supplementary Fig. 5d). To confirm whether TaPIR1 can catalyze the ubiquitination of these sites, we expressed and purified TaHRP1 mutants and performed an *in vitro* ubiquitination assay. When the lysine residues K¹³¹ and K¹³⁶ were mutated into the arginine residues R¹³¹ and R¹³⁶, respectively, the extent of ubiquitination of TaHRP1^{K131R} and TaHRP1^{K136R} was not significantly different compared with that of TaHRP1 (Fig. 2e). In contrast, TaHRP1^{K131,136R} ubiquitination remained inconspicuous (Fig. 2e). We also evaluated the ubiquitination of three mutants of TaHRP1 *in vivo*. Western blotting analysis of proteins eluted from GFP-trap beads revealed some amount of ubiquitinated TaHRP1^{K131R} and TaHRP1^{K136R} but not of ubiquitinated TaHRP1^{K131,136R} upon their transient expression

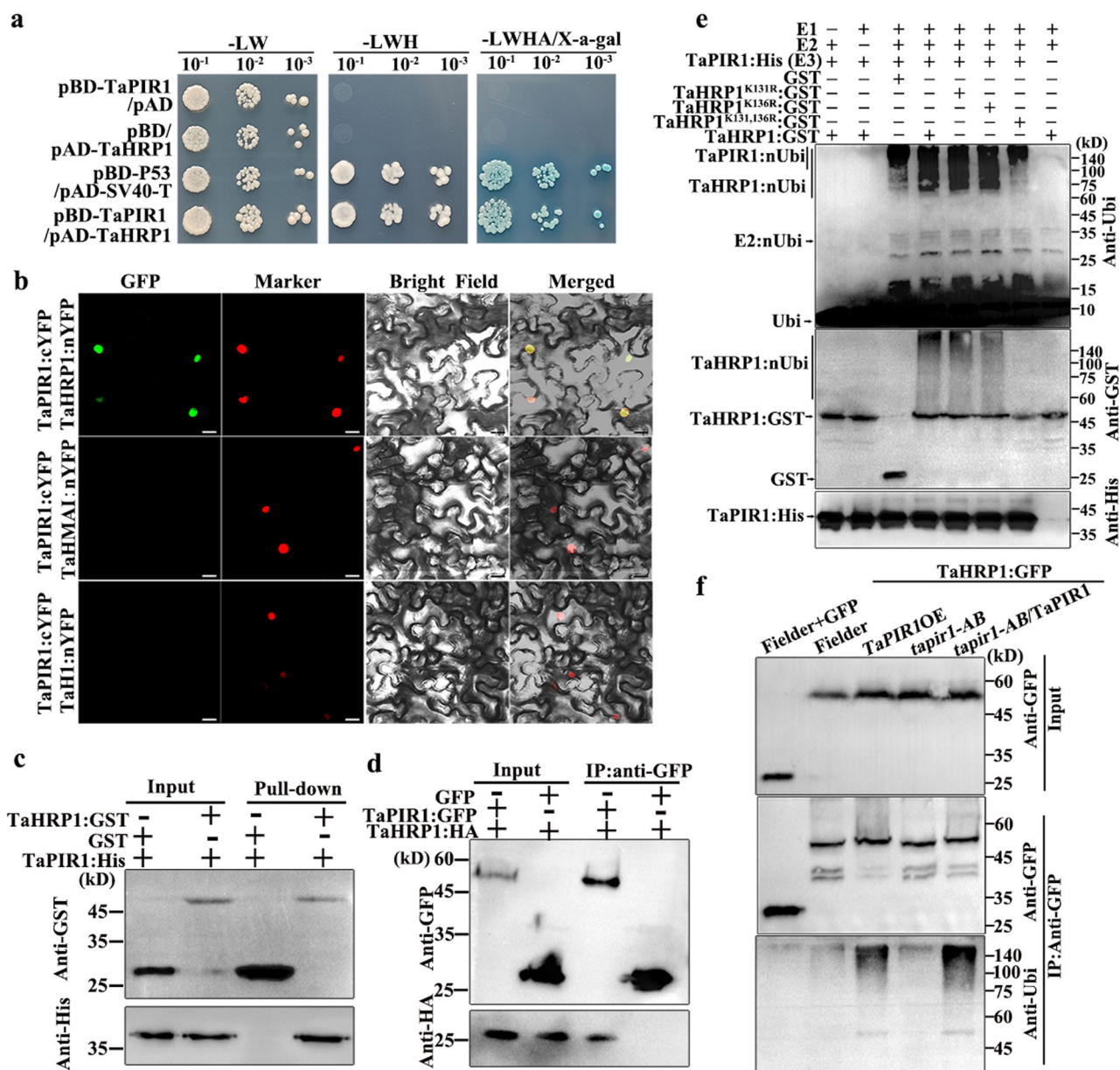


Fig. 2 | TaPIR1 interacts with and ubiquitinates TaHRP1 in vivo. **a** Detection of TaPIR1–TaHRP1 interaction using the yeast two-hybrid assay. Yeast transformants with marked constructs were grown on SD medium lacking LW (-Leu/-Trp) and those with LacZ activities were grown on SD-LWHA (-Leu/-Trp/His/-Ade) supplemented with X- α -gal. **b** Detection of TaPIR1–TaHRP1 interaction in the nucleus of *N. benthamiana* leaves expressing the corresponding constructs based on the BIFC assay. A NLS fused with a red fluorescent protein (RFP) was used as a nucleus marker. Bar = 20 μ m. Similar results are obtained from two independent biological experiments. **c** Verification of TaPIR1–TaHRP1 interaction using GST pull-down assay. Western blots of the recombinant protein mixture and proteins eluted from GST beads were detected with anti-His or anti-GST antibodies. Similar results are obtained from three independent biological experiments. **d** Confirmation of the TaPIR1–TaHRP1 interaction via Co-IP assays. Total proteins from *N. benthamiana*

leaves expressing the labeled constructs and proteins copurified from GFP beads were detected via western blotting with anti-GFP and anti-HA antibodies. Similar results are obtained from two independent biological experiments.

e Ubiquitination of TaHRP1 by TaPIR1 in vitro. Ubiquitinated TaHRP1, GST-tagged TaHRP1, and His-tagged TaPIR1 were separated and detected via western blotting with anti-ubiquitin, anti-GST, and anti-His antibodies, respectively. Similar results are obtained from two independent biological experiments. **f** Confirmation of TaHRP1 ubiquitination by TaPIR1 in protoplasts prepared from *tapir1-AB*, TaPIR1-overexpression, *tapir1-AB*-expressing *TaPIR1* and Fielder plants. Ubiquitinated proteins copurified from the total proteins were detected with an anti-ubiquitin antibody. Similar results are obtained from two independent biological experiments. Source data are provided as a Source Data file.

in tobacco (Supplementary Fig. 5e). To exclude the possibility of a relationship between three TaHRP1 mutants and TaPIR1 may influence ubiquitination of TaHRP1, these interactions were analyzed through the Y2H assays. Similar to TaHRP1, three mutants were found to interact with TaPIR1 (Supplementary Fig. 4f). These results demonstrate that TaPIR1 can ubiquitinate the K¹³¹ and K¹³⁶ residues of the TaHRP1 protein.

To further determine the key lysine sites responsible for TaHRP1 stability, we conducted a cell-free degradation assay to detect the stability of three mutants of TaHRP1 by incubating total protein extracts from *tapir1-AB*, WT, and *TaPIR1*-overexpressing plants, respectively. When incubated with WT or *TaPIR1*-overexpressing plant extracts, the degradation rates of TaHRP1^{K136R}:GST and TaHRP1^{K131R}:GST increased but remained relatively stable in incubation mixtures

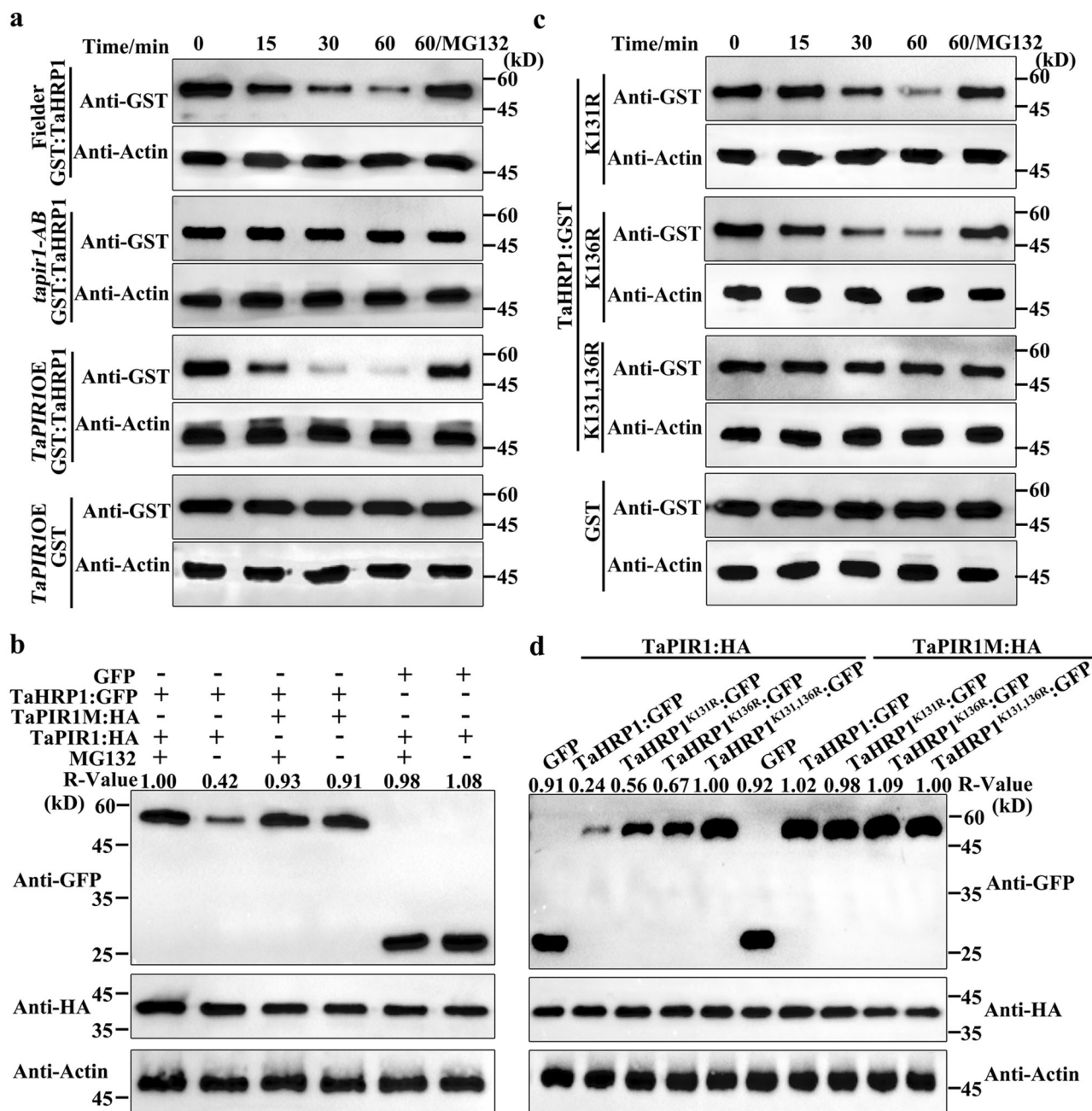


Fig. 3 | TaPIRI-induced TaHRP1 degradation depends on the lysine residues K¹³¹ and K¹³⁶ of TaHRP1. a Cell-free degradation assay of TaHRP1 in coincubation mixtures from Fielder (WT), *tapir1-AB*, and *TaPIRIOE* plants. TaHRP1:GST derivatives expressed and purified in *E. coli* were incubated for different times at 28 °C with protein extracts from Fielder (WT), *tapir1-AB*, and *TaPIRIOE*-overexpressing plant leaves. The relative intensities (*R*-value) of each band were evaluated using ImageJ software and are shown above the bands. The bands in the left electrophoresis line are reference bands (set to 1). **b** In vivo degradation of TaHRP1 in *N. benthamiana* leaves transiently expressing *TaPIRI*. Protein levels were detected via western blotting with anti-GFP antibody in the presence of 50 μM MG132 or an equal volume of DMSO (control). The relative intensities (*R*-value) of each band are shown above

the bands, and the bands in the left electrophoresis line are used as a reference (set to 1). Actin was used as the loading control. **c** Cell-free degradation assay of mutants of TaHRP1 detected in coincubation mixtures from Fielder (WT) incubated for different times at 28 °C. The relative intensities (*R*-value) of each band are shown above the bands, and the bands in the left electrophoresis line are reference bands (set to 1). Actin was used as the loading control. **d** Mutants of TaHRP1 in vivo accumulation assay. Different mutants of TaHRP1 were coexpressed with *TaPIRI* in *N. benthamiana* leaves. The relative intensities (*R*-value) of each band are shown above the bands, and the bands in the right electrophoresis line are used as a reference (set to 1). Actin was used as the loading control. Source data are provided as a Source Data file.

from *tapir1-AB* plant (Fig. 3c and Supplementary Fig. 6). In contrast, TaHRP1^{K131,136R} remained relatively stable in all coincubation mixtures (Supplementary Fig. 6). Repeated experiments revealed TaPIR1, but not TaPIR1M, significantly promoted TaHRP1^{K131R} and TaHRP1^{K136R} protein degradation when three mutants of TaHRP1 and TaPIR1 or TaPIR1M was transiently co-expressed in *N. benthamiana* (Fig. 3d). No changes were observed in TaHRP1^{K131,136R} protein abundance (Fig. 3d).

Overall, these findings consistently demonstrate that TaPIRI ubiquitinates K¹³¹ and K¹³⁶ sites of TaHRP1 protein, thereby mediating its degradation.

TaHRP1 is a positive regulator of wheat resistance to *Pst*

To determine the role of TaHRP1 in *Pst* infection, we first conducted CRISPR-Cas9-mediated gene editing to fully edit three *TaHRP1*

homologs in the wheat cultivar Fielder. Subsequently, we identified a *tahrp1* line in which three *TaHRP1* homologs contained deletions leading to frameshift mutations (Supplementary Fig. 2d). Upon infection with avirulent *Pst* CYR23, a typical resistance response with HR was observed in Fielder plants; in contrast, *tahrp1* plants presented with evident urediniospore pustules (Fig. 4a). *TaPR1* and *TaPR2* transcription was reduced 2–4-fold at 0 hpi and 24 hpi in *tahrp1* plants compared with that in Fielder plants (Supplementary Fig. 7a, b). Consistently, *tahrp1* plants showed >50–60% increase in fungal biomass relative to the controls (Fig. 4b). Moreover, histochemical examination of *Pst* revealed longer hyphae and larger infection areas in the *tahrp1* plant than in the control (Fig. 4c). In repeated experiments, the hyphal length and infection areas of *Pst* CYR23 increased compared with the control (Fig. 4d, e). These results confirm that the loss of *TaHRP1* markedly reduces resistance to avirulent *Pst*.

To further determine the role of *TaHRP1* in wheat stripe rust resistance, we generated transgenic wheat lines overexpressing *TaHRP1* (*TaHRP1OE*). The transcript levels of *TaHRP1* in *TaHRP1OE*#L3 and #L5 plants increased threefold and fourfold, respectively (Supplementary Fig. 2e). YFP-tagged *TaHRP1* was also detected via western blotting with an antibody against GFP, indicating the successful expression of *TaHRP1* in *TaHRP1OE*#L3 and #L5 plants (Supplementary Fig. 2f). When inoculated with virulent *Pst* CYR34, Fielder plants developed numerous urediniospore pustules and showed no obvious HR at 14 dpi, whereas *TaHRP1OE*#L3 and L5 plants developed sporadic urediniospore pustules and showed HR (Fig. 4f). *TaHRP1OE*#L3 and L5 plants showed 40–50% reduction in *Pst* biomass at 120 hpi relative to WT plants (Fig. 4g). In addition, we measured the expression of two defense-related genes in transgenic wheat lines overexpressing *TaHRP1*. *TaPR1* and *TaPR2* expression increased 2–3-fold at 0 hpi and 24 hpi in the *TaHRP1OE*#L3 and L5 plants compared with that in Fielder plants (Fig. 4h). Taken together, *TaHRP1* may function as a positive regulator of wheat stripe rust resistance.

TaHRP1 acts as a transcription factor directly targeting PhANGs

As *TaHRP1* is homologous to the forkhead box protein B2 that binds to a cis-acting element²⁷, we hypothesized that *TaHRP1* acts as a transcription factor in the nucleus. To test this hypothesis, we first confirmed the predicted NLS in the C-terminal region. Upon transient expression of *TaHRP1*:GFP in *N. benthamiana*, GFP signals were predominantly observed in the nucleus, with only a portion of *TaHRP1*:GFP accumulating in the cytoplasm (Supplementary Fig. 8a, b). Similar results were confirmed in the nuclear extracts of *N. benthamiana* leaves transiently expressing *TaHRP1*:GFP. A high accumulation of *TaHRP1*:GFP was detected on the western blots of proteins isolated from the plant nucleus (Supplementary Fig. 8c).

Next, we assessed the self-transactivation activity of *TaHRP1* in yeast. Yeast cells expressing pBD:*TaHRP1* were cultured on SD-His plates supplemented with 25 mM 3-AT and exhibited galactosidase activity (Supplementary Fig. 8d). To identify the self-transactivation activity region, two different fragments of *TaHRP1* were amplified and tested in yeast cells. The self-transactivation activity of *TaHRP1* was eliminated after the C-terminal region was deleted but not after the deletion of the histidine-rich region, indicating that the C-terminal region of *TaHRP1* is required for its self-transactivation activity (Supplementary Fig. 8d).

Based on the Y2H assay, the *TaHRP1* was found to interact with itself, indicating its homodimer-forming ability (Supplementary Fig. 9a). When the cysteine residue C⁴⁶ was mutated into an alanine residue in *TaHRP1*, the mutant *TaHRP1*^{C46A} eliminated its interaction with *TaHRP1* (Supplementary Fig. 9a). Subsequently, we performed Co-IP and split-luciferase complementation imaging assays to further confirm the *TaHRP1*–*TaHRP1* interaction (Supplementary Fig. 9b, c). In addition, the BIFC assay revealed that the homointeraction between *TaHRP1* and *TaHRP1* mainly occurred in the plant nucleus

(Supplementary Fig. 9d). The purified *TaHRP1* protein was then analyzed via native polyacrylamide gel and immunoassay to detect *TaHRP1* oligomerization. In the absence of β -mercaptoethanol (β -ME), the *TaHRP1* oligomers were detected but the *TaHRP1*^{C46A} mutant could not undergo oligomerization (Supplementary Fig. 9e).

To further identify *TaHRP1*-regulated target genes, DNA affinity purification sequencing (DAP-seq) was employed to determine its genome-wide binding sites. Overall, 4.43%, 88%, and 2.74% of *TaHRP1*-binding peaks were distributed in promoter, intergenic, and intron regions, respectively (Supplementary Fig. 10a). We identified 27,876 and 17,839 loci, with an overlap of 5440 target peaks (Supplementary Fig. 10b). *TaHRP1*-binding peaks were enriched around the transcription start sites, indicating that these peaks are strongly enriched in promoter regions (Supplementary Fig. 10c). Motif enrichment analysis of the *TaHRP1*-binding peaks revealed that the AAGAAGAAG element (e -value = $6.3e-2067$) was the most enriched motif in both DAP-seq replicates, hereafter named as HBS (Fig. 5a). KEGG analysis revealed that the potential *TaHRP1*-binding genes involved in photosynthesis were markedly enriched, among which four encode PSII proteins (*PsbI-1A*, *PsbE-2D*, *PsbE-5D*, and *PsbD-4D*), three encode cytochrome b6f subunits (*PetA-3B*, *PetN-6B*, and *PetN-2D*), four encode PSI proteins (*PsaI-7D*, *PsaI-1A*, *PsaA-2B*, and *PsaA-3B*) and one encodes ATP synthase subunit (*AtpH-4A*) (Fig. 5b). The heatmap revealed that, compared with the control, the DNA-binding peaks of the above-mentioned PhANGs were enriched by *TaHRP1* in the two DAP-seq replicates (Fig. 5c). Consistently, visual assessment of the binding peaks of PhANGs confirmed that the notable conspicuous peaks were present in their promoter regions (Fig. 5d and Supplementary Fig. 10d). These results indicate that *TaHRP1* may regulate the expression of PhANGs.

TaHRP1 regulates PhANG expression

DAP-seq revealed that the promoter region exhibited considerable enrichment of PhANGs. To validate the reliability of our DAP-seq results, the promoter fragment of *PsbE-2D* containing the HBS element was isolated and incubated with the *TaHRP1*:GST protein using the electrophoretic mobility shift (EMSA) assays. Evidently, a specific band appeared only when *TaHRP1*:GST was included. With an increase in *TaHRP1*:GST concentration, a band indicative of binding increased in abundance, whereas the band was completely absent in the HBS element-mutated probe control (Fig. 5e and Supplementary Fig. 11a). However, all histidine residues in the histidine-rich domain in the N-terminal region of *TaHRP1* mutated into alanine (*TaHRP1*^{H/A}), eliminating its interaction with the HBS DNA probe (Supplementary Fig. 11b). We further examined the thermodynamics of *TaHRP1*–HBS interaction using isothermal titration calorimetry (ITC). When the HBS element was injected into cell pools containing GST and *TaHRP1*^{H/A}:GST proteins, the heat exchange volumes were small and could not fit any binding model, indicating that there was no specific binding between the HBS element and GST or *TaHRP1*^{H/A}:GST (Supplementary Fig. 11c). In contrast, considerable heat changes were observed upon injecting the HBS element into cells containing *TaHRP1*:GST protein (Supplementary Fig. 11c). The binding constant (Kd) values were determined to be $0.14 \pm 0.08 \mu\text{M}$ for *TaHRP1*:GST and $0.36 \pm 0.15 \text{ mM}$ for *TaHRP1*^{H/A}:GST, suggesting that the histidine-rich domain in the N-terminal region of *TaHRP1* is essential for its interaction with HBS (Fig. 5f).

To investigate the mechanism through which *TaHRP1* regulates PhANGs expression, we subsequently performed a dual-luciferase reporter assay to determine the effect of *TaHRP1* on the transcription of 12 PhANGs. The results revealed that the expression of four PSII-related genes (*PsbI-1A*, *PsbD-4D*, *PsbE-5D*, and *PsbE-2D*), three ETC-related genes (*PetA-3B*, *PetN-2D*, and *PetN-6B*), and one *AtpH-4A* gene was significantly transactivated by *TaHRP1*, with the expression of four PSI-related genes (*PsaI-7D*, *PsaI-1A*, *PsaA-3B*, and *PsaA-2B*) remaining unaffected compared with that of the control (Fig. 6a). To assess the impact of *TaHRP1* on *TaHRP1*-mediated transcriptional regulation of

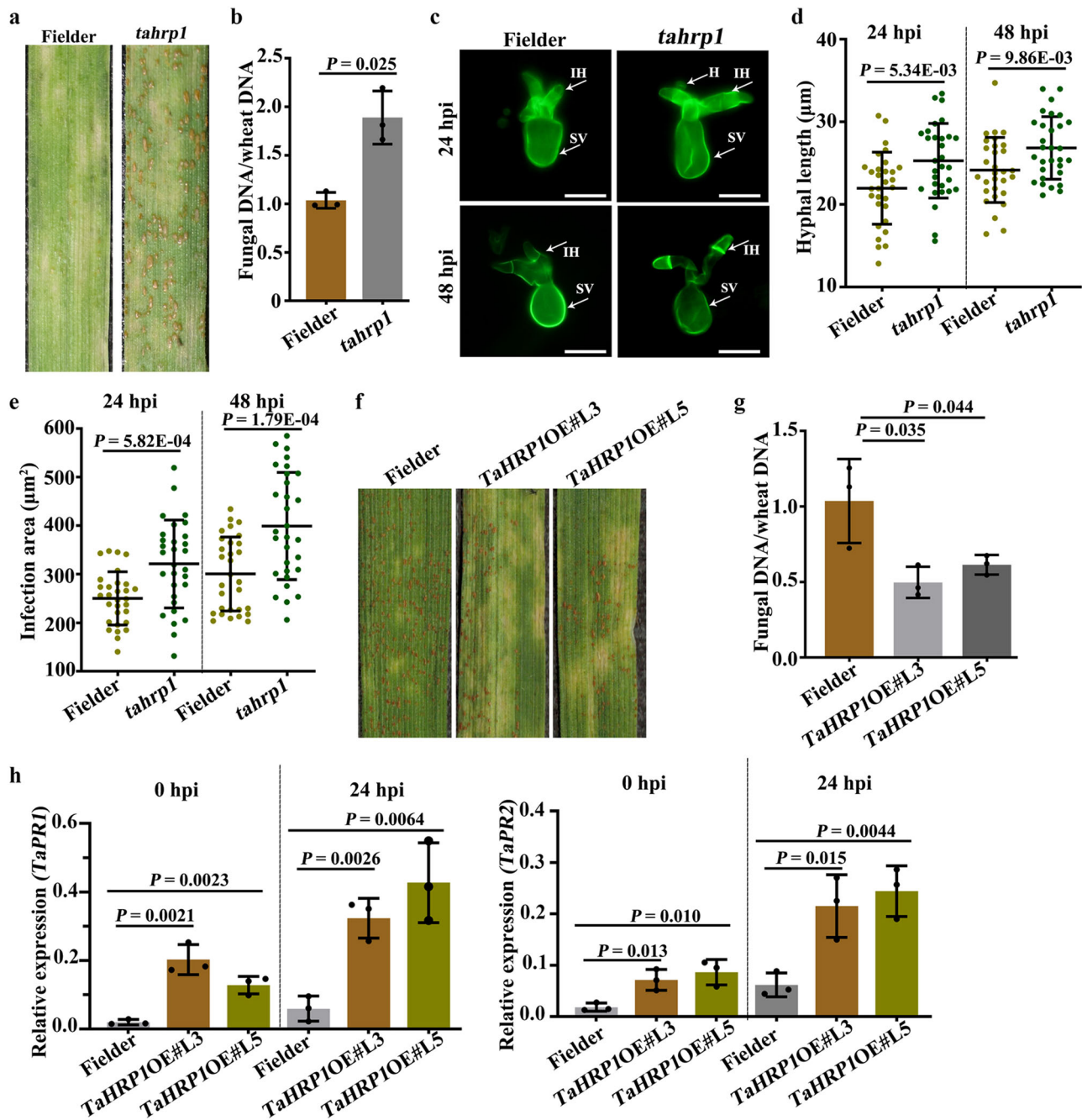


Fig. 4 | TaHRP1 contributes to resistance to *Pst* in wheat. **a** The second leaves of the seedlings of the T₂ generation of *tahrp1* and Fielder plants were inoculated with *Pst* CYR23. Leaves infected with *Pst* urediniospores were observed at 14 dpi. **b** The biomass ratio (*Pst*/wheat) was measured using DNA isolated from the second leaves inoculated with *Pst* at 120 hpi. Wheat *TaEF* and rust *PstEF* were used to normalize the DNA level. Values are mean \pm SD, $n = 3$ biologically independent samples. Data was analyzed using an unpaired two-tailed Student's *t*-test. **c** *Pst* growth and development in *tahrp1* and Fielder plants inoculated with *Pst* CYR23 at 24 hpi and 48 hpi. Representative images were observed using CellSens Entry software. IH infectious hyphae, SV substomatal vesicle, bar = 20 μ m. **d**, **e** Hyphal length and infection areas were analyzed using CellSens Entry software at 24 hpi and 48 hpi. Means \pm SD were calculated from 30 infection sites of three independent biological

repeats. The *P* value was determined by a two-tailed unpaired Student's *t*-test. **f** *Pst* uredinia on the second leaves of *TaHRP1OE* and Fielder's plants inoculated with *Pst* CYR34 were obtained at 14 dpi. **g** Fungal biomass at 14 dpi with *Pst* CYR34 was determined via qPCR. *TaEF* and *PstEF* were used as internal control genes to measure wheat and *Pst* DNA with reference to the standard curves. Values are mean \pm SD, $n = 3$ biologically independent samples. The *P* value was determined by a two-tailed unpaired Student's *t*-test. **h** Relative expression of the marked defense-related genes in *TaHRP1OE* plants at 0 hpi and 24 hpi with *Pst* CYR34. Transcript levels were confirmed via qRT-PCR and normalized with *TaEF*. Values are mean \pm SD, $n = 3$ biologically independent samples. The *P* value was determined by a two-tailed unpaired Student's *t*-test. Source data are provided as a Source Data file.

PhANGs, we used TaHRP1 as an effector in the dual-luciferase reporter assay of *N. benthamiana* leaves expressing TaPIR1:GFP and TaPIRIM:GFP. Transient expression of TaPIR1:GFP, but not TaPIRIM:GFP, suppressed the downstream activation of TaHRP1 (Fig. 6b). These conclusions were further supported by qRT-PCR

results revealing the increased expression of four PSII-related genes and three ETC-related genes in *tapir1-AB* transgenic wheat compared with that in the controls, whereas reversed expression pattern was observed in Fielder plants expressing *TaPIR1* (Supplementary Fig. 12a, b). In addition, the transcripts of PSII-related genes and ETC-related

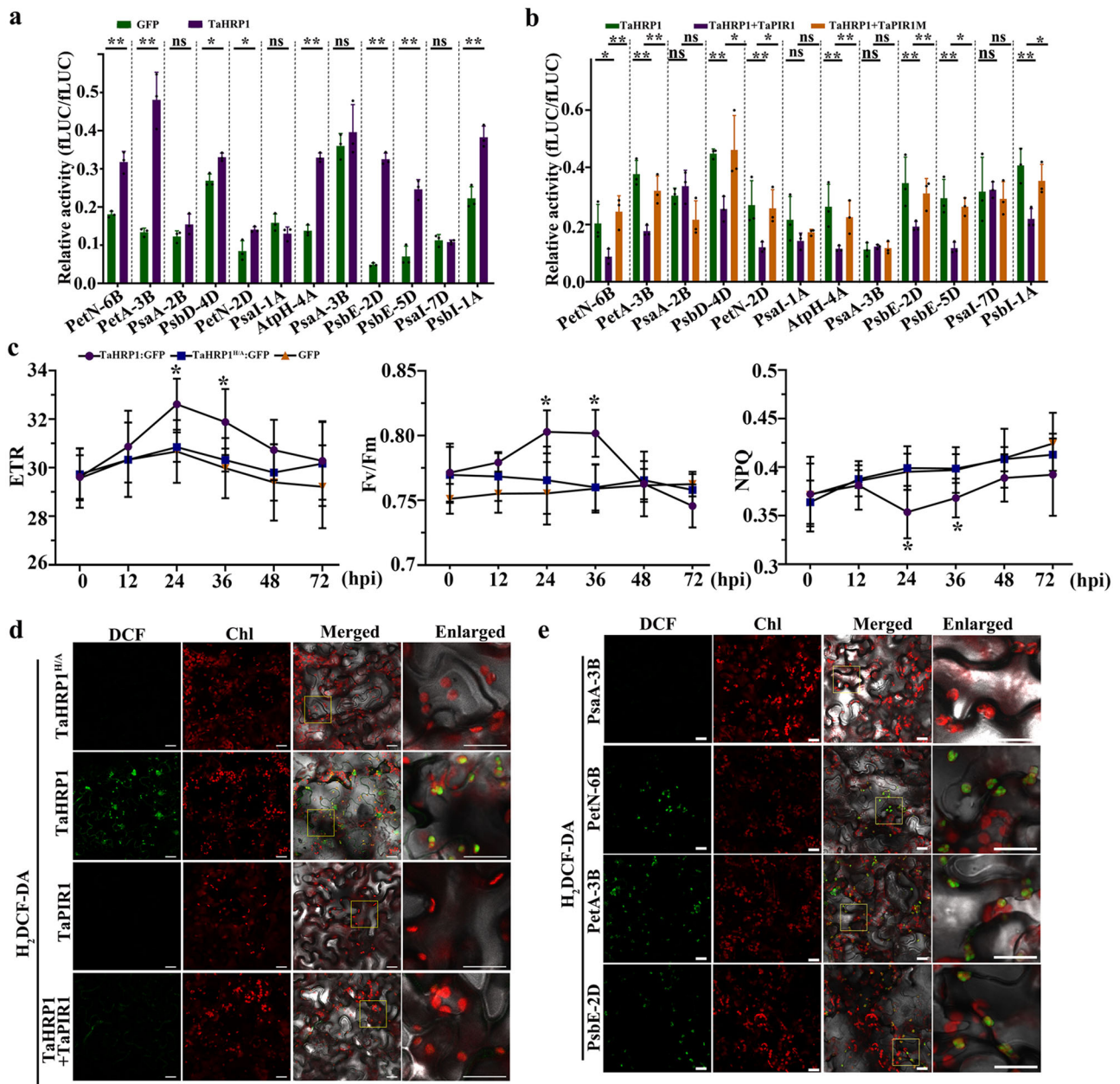


Fig. 6 | TaHRP1 induces chloroplast-derived ROS accumulation by activating PhANGs. **a** Dual-luciferase reporter assay showed that the transcriptional activities of PhANGs were activated by TaHRP1. The corresponding reporter and effector constructs were simultaneously transformed into *N. benthamiana* leaves, and the enzyme activities of firefly luciferase (LUC) and Renilla luciferase (REN) were detected at 48 hpi. Data are presented as the mean \pm SD of three biological replicates. The *P* value was determined by a two-tailed unpaired Student's *t*-test. **b** Suppression of TaHRP1-activated PhANGs expression in *N. benthamiana* leaves transiently expressing *TaPIR1*. Data are presented as the mean \pm SD of three biological replicates. The *P* value was determined by a two-tailed unpaired Student's *t*-test for multiple comparisons. **c** Assays for electron transport rate (ETR), maximum dark-adapted quantum efficiency (Fv/Fm), and nonphotochemical quenching

(NPQ) in *N. benthamiana* leaves infiltrated with *Agrobacterium* expressing TaHRP1, TaHRP1^{H/A}, or GFP. Data are presented as the mean \pm SD of three biological replicates. The *P* value was determined by a two-tailed unpaired Student's *t*-test.

d Suppression of TaHRP1-induced ROS in chloroplasts by TaPIR1. Tobacco leaves infiltrated with *Agrobacterium* expressing TaHRP1 and TaPIR1, TaHRP1^{H/A}, TaPIR1 alone (control), or TaHRP1 treated with H₂DCF-DA were observed for DCF signals. Bar = 20 μ m. Similar results are obtained from three independent biological experiments. **e** *N. benthamiana* leaves treated with H₂DCF-DA were observed via confocal microscopy for DCF signals at 48 hpi with *Agrobacterium* strains expressing PhANGs. Bar = 20 μ m. Similar results are obtained from three independent biological experiments. Source data are provided as a Source Data file.

TaHRP1-overexpression wheat plants, the ETR was increased compared with the ETR in Filderer plants (Supplementary Fig. 7c). These results indicate that TaHRP1 plays a significant role in modulating photosynthesis.

As ROS are unavoidable byproducts of photosynthesis and are mainly generated in chloroplasts, we measured chloroplast-derived ROS accumulation using the probe 2',7'-dichlorodihydrofluorescein

diacetate (H₂DCF-DA) in tobacco leaves and wheat protoplasts overexpressing TaHRP1^{H/A}, TaHRP1, and TaPIR1. Notably, TaHRP1 induced a high accumulation of ROS in chloroplasts but TaHRP1^{H/A} or TaPIR1 did not exert the same effect (Fig. 6d and Supplementary Fig. 13a). Importantly, more ROS was accumulated in wheat protoplasts of TaHRP1OE and tapir1-AB plants, whereas no ROS accumulation was observed in wheat protoplasts of WT, tahrp1, or TaPIR1-overexpressing

plants (Supplementary Fig. 13b). In addition, we measured ROS production in *TaHRP1OE* plants inoculated with *Pst* CYR34, which revealed that H₂O₂ accumulation increased at 24 hpi and 48 hpi (Supplementary Fig. 13c, d). Furthermore, the influence of TaPIR1 on TaHRP1-induced ROS production was detected. Transient coexpression of *TaHRP1* and *TaPIR1* in tobacco gradually reduced TaHRP1-induced ROS production (Fig. 6d). To verify that ROS production was induced by PhANGs expression, we also examined ROS production in *N. benthamiana* leaves transiently expressing PhANGs. The DCF signal was strongly enhanced in leaves transiently expressing *PetN-6B*, *PetA-3B*, *PsbE-2D*, *PsbI-1A*, *PsbE-5D*, *PsbD-4D*, and *AtpH-4A* (Fig. 6e and Supplementary Fig. 14). No significant difference in the oxidized DCF signal was observed in the leaves expressing *PsaA-3B* and *PsaI-7D* (Fig. 6e and Supplementary Fig. 14). Therefore, TaHRP1 may contribute to photosynthesis and ROS production in chloroplasts to activate plant immunity, possibly by modulating PhANGs expression.

Discussion

The ubiquitin/proteasome pathway is a crucial protein quality control system in eukaryotes. There is substantial evidence to support that protein ubiquitination is an important component of regulatory networks controlling various plant cellular processes, including growth and development, as well as defense responses, such as APIP6 and RIP1 in rice^{23,29,30}. However, there are limited reports of protein ubiquitination in wheat immunity responses to microbial pathogens. In this study, transcriptome sequencing of *Pst*-infected wheat leaves revealed that the expression of the gene encoding the E3 ligase *TaPIR1* was highly induced at early infection stages. Simultaneous gene editing of *TaPIR1* via CRISPR-Cas9 enhanced resistance to stripe rust in wheat, indicating that TaPIR1 is an important positive regulator of wheat susceptibility to *Pst*. In addition, to hinder nutrient uptake for pathogen development, fungal colony areas and hyphal growth were restricted in *tapir1-AB* wheat plants with an increase in ROS accumulation at infection sites. Modification of susceptibility genes has been widely regarded an effective measure to confer broad-spectrum and durable resistance in plants^{31,32}. Mildew resistance locus O (MLO) was modified to enhance plant resistance to powdery mildew, and a 304-kbp targeted deletion in the MLO-B1 locus conferred robust powdery mildew resistance while maintaining wheat growth and yield³³. The wheat kinase gene *TaPslPKI*, a susceptibility gene, has been identified as an ideal target for inducing broad-spectrum resistance to rust in wheat³⁴. Another study showed that the knockout of three homoalleles of *TaWRKY19* improved the TaNOX10-mediated ROS burst and conferred high resistance to *Pst*³⁵. Therefore, TaPIR1 may act as a genetic engineering target to provide durable resistance to this disease-causing pathogen.

TaPIR1 was shown to physically interact with the histidine-rich protein TaHRP1 in the plant nucleus, which has not been functionally characterized in wheat. We revealed that TaPIR1 acts as a typical RING-finger domain-containing E3 ligase to ubiquitinate the K³¹ and K¹³⁶ residues of TaHRP1 protein and modulate its stability. Interestingly, TaHRP1 does not contain any known domains, except for a histidine-rich motif at its N-terminal region. Our results demonstrated that a histidine-rich motif is essential for binding to a cis-acting element as a transcription factor. Previous studies on *Citrus unshiu* have shown that the histidine-rich domains of dehydrin CuCOR15 contributed to the binding of DNA and metals, including Fe³⁺, Cu²⁺, and Zn²⁺^{36,37}. Deletion of the histidine-rich motif of dehydrin OpsDHN1 in *Opuntia streptacantha* did not affect its dimer formation but suppressed its import into the nucleus³⁸. Based on the results of this study, we speculated that TaHRP1 acts as an atypical transcription factor with an activation domain at the C-terminal region and a DNA-binding domain at the N-terminal region. TaHRP1 overexpression in wheat plants was shown to promote ROS accumulation and exert a strong positive effect on plant resistance to *Pst*; however, the loss of function of *TaHRP1* in

wheat resulted in reduced plant resistance. During pathogen invasion in plants, instantaneous ROS bursts in plant tissues can induce programmed cell death to inhibit pathogen growth and development. Therefore, we speculate that the E3 ligase TaPIR1 suppresses ROS accumulation to confer wheat susceptibility to *Pst* via direct ubiquitination and degradation of the positive factor TaHRP1.

In addition to supplementing photosynthesizing tissues with carbon sources and energy, chloroplasts are hubs for plant-pathogen interaction^{39,40}. A reduction in the expression of PsbD (a PSII subunit) regulated by the transcription factor TPC13 was compromised in the ETI of *Hyaloperonospora arabidopsidis*^{41,42}. Our results revealed that TaHRP1 overexpression promoted Fv/Fm and ETR and exerted a positive effect on plant photosynthesis. TaHRP1 activated PhANGs expression to encode core elements of PSII, cytochrome b6f complex, and ATP synthase⁴³. Overexpression of the ATP synthase α -subunit gene reduced the viral load in both *N. benthamiana* and soybean plants. In several plant-pathogen interactions, reduced photosynthesis in susceptible plants promotes pathogen spread and colonization, but some resistant plants exhibit increased expression of photosynthesis-related genes in response to pathogen invasion⁴⁴. Earlier studies have shown that low expression levels of the cytochrome b/f complex in transgenic tobacco can impair electron transport and reduce the CO₂ assimilation rate⁴⁵. The cytochrome b6/f complex and ATP synthase are considered crucial factors in the reduction of electron transport and photosynthetic capacity⁴⁶. Thus, we speculate that TaHRP1 affects the photosynthetic capacity to enhance plant defense by increasing the number of core protein complexes in the photosynthetic system. Maintaining high levels of photosynthesis is important to protect PSII and PSI from damage by ROS and excess light. There is an urgent need to increase the demand for photosynthesis to provide the energy required for defense responses, which contributes to plant biosynthesis and metabolism to generate phytohormones, secondary metabolites, and defense-related proteins when organisms encounter pathogen invasion²⁸. Furthermore, the induction of chloroplast photosynthesis genes induces hormone signaling pathways that partially contribute to local and systemic resistance to pathogens⁴⁷.

Increasing evidence has shown that inhibition of photosynthesis is stock-in-trade for the suppression of plant immunity, leading to bacterial, viral, and fungal multiplication⁴⁸⁻⁵⁰. To suppress chloroplast function, the photosynthetic apparatus in plant immunity is usually targeted by pathogen-secreted virulence factors, such as HopN1 and Pst_12806⁵¹⁻⁵³. The HopN1 from *Pseudomonas syringae* and Pst_12806 from rust fungi can interact with plant PsbQ (a protein present in the oxygen-evolving complex of PSII) and ISP, respectively, to suppress chloroplast-derived ROS accumulation^{51,53}. The interference of pathogens with photosynthetic functions may explain why different components in the photosystem play an important role in precisely regulating chloroplast-derived ROS accumulation for plant immunity. A high ISP level can improve the photosynthetic ETR and induce ROS overproduction in PETC⁵¹. Our results showed that transient expression of TaHRP1 and its target PhANGs-related PETC promote chloroplast-derived H₂O₂ accumulation. However, increased levels of PsaI and PsaA, two reaction centers of PSI, failed to induce ROS in chloroplasts. In fact, the PETC and PSII of chloroplasts produce the largest pools of ROS. By contrast, the level of ROS does not change significantly in PSI reaction center^{54,55}. Excessive ROS accumulation can accelerate chlorophyll degradation, lipid peroxidation, and photosynthesis reduction by oxidative damage to the photosystem, resulting in cell death⁵⁶. Therefore, we speculate that TaHRP1 enhances photosynthetic capacity by activating PhANGs, resulting in excessive light absorption by PSII. This excess energy might be transferred from chlorophyll to molecular oxygen for ROS accumulation.

In summary, our results indicate a susceptible mechanism in which the E3 ligase TaPIR1 ubiquitinates and degrades the transcription factor TaHRP1, attenuates TaHRP1-regulated PhANGs expression,

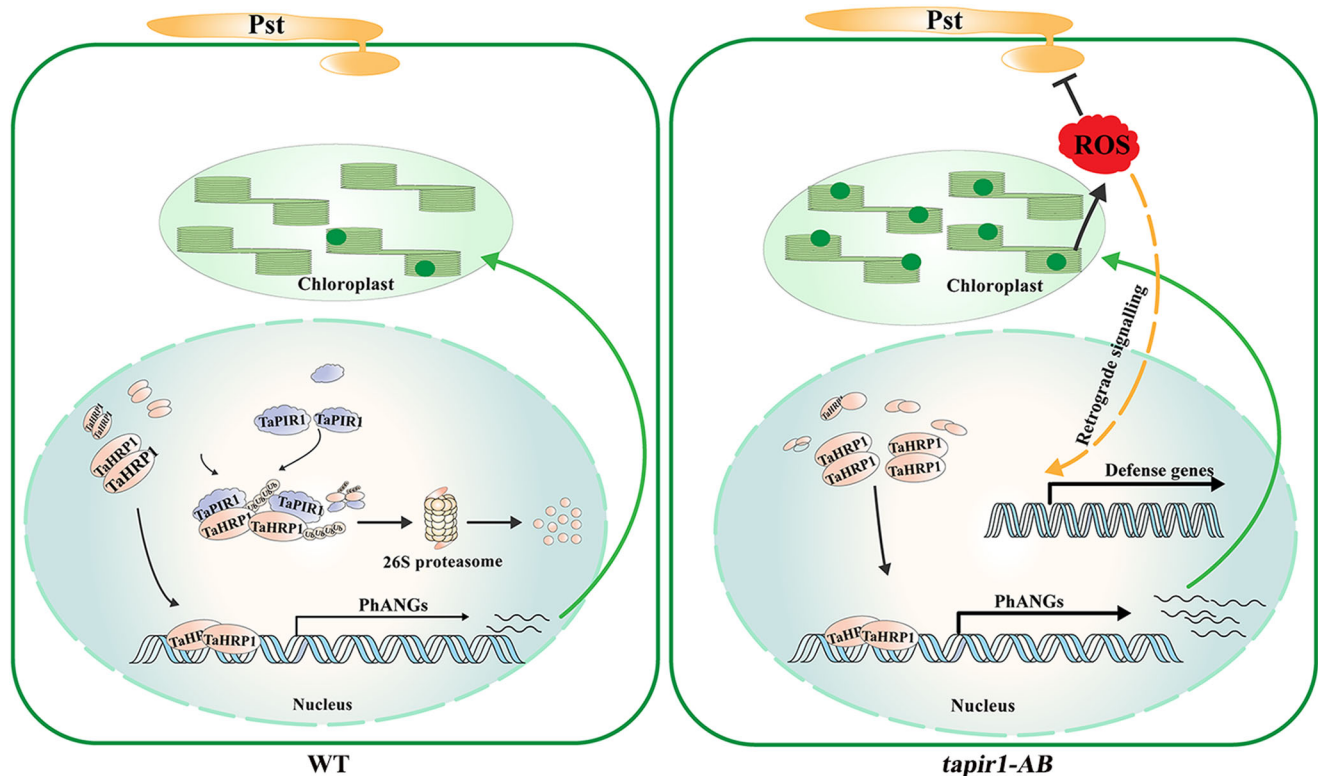


Fig. 7 | Working model of the role of the TaPIR1-TaHRP1 cascade during *Pst*-wheat interaction. The RING-finger ubiquitin E3 ligase TaPIR1 is translocated into the plant nucleus, where it interacts with and ubiquitinates the atypical transcription factor TaHRP1. TaPIR1-TaHRP1 interaction and modification promote

TaHRP1 degradation and interfere with TaHRP1-induced PhANGs expression, resulting in attenuated chloroplast-derived ROS accumulation. In *tapir1-AB* plants, TaHRP1 accumulation activates PhANGs expression and induces ROS accumulation, which contributes to resistance to *Pst* in wheat.

and decreases chloroplast-derived ROS accumulation (Fig. 7). During wheat-*Pst* interaction, when *TaPIR1* expression was induced by virulent *Pst*, TaPIR1 directly ubiquitinated TaHRP1 to promote its degradation, which further inhibited chloroplast-derived ROS accumulation due to low expression levels of TaHRP1-regulated PhANGs, thus compromising wheat immunity. In contrast, in *tapir1-AB* plants, high TaHRP1 accumulation enhanced the expression of PhANGs transcripts to promote chloroplast-derived ROS accumulation and photosynthesis, which restricted infection and conferred host resistance.

Methods

Experimental materials and growth conditions

Wheat seedlings and *N. benthamiana* were grown in a greenhouse at 16 °C and 23 °C, respectively, under a light/dark photoperiod of 16 h/8 h. Wheat cultivar Fielder was used to establish *TaPIR1* knockout (*tapir1-A* and *tapir1-AB*) plants, *TaHRP1* knockout (*tahrp1*) plants, and *TaHRP1* overexpression (*TaHRP1OE*) plants. For inoculation with *Pst* races CYR23, CYR31, and CYR34, wheat seedlings were grown and inoculated with urediniospores of *Pst* at 16 °C under a light/dark photoperiod of 16 h/8 h⁵⁷. For transgenic wheat tillering and seed collection, the plant seeds from all backgrounds were grown at 25 °C with a photoperiod of 16 h of light and at 20 °C with 8 h of dark. *A. tumefaciens* (GV3101 and EHA105) and *E. coli* (DH5a and BL21) were stored at -80 °C and cultured in Luria-Bertani medium at 28 °C and 37 °C, respectively. The yeast strain (AH109) was cultured at 30 °C for the Y2H assays.

Construction of transgenic wheat lines

To perform CRISPR-Cas9 editing of *TaPIR1* and *TaHRP1*, two candidate gRNAs targeting three copies of these genes were designed, and their editing efficiencies were determined using WheatOmics (<http://202>

194.139.32)⁵⁸. These gRNAs exhibiting high efficiency were introduced into the pBUE411 vector to establish the CRISPR-Cas9 vector. The *A. tumefaciens* strain EHA105 harboring the recombinant vector was transformed into immature embryos of the wheat cultivar Fielder via *Agrobacterium*-mediated transformation⁵⁹. The genomic DNA of the positive transgenic seedlings was extracted for PCR detection of the Cas9 gene fragment. For constructing TaHRP1-overexpressing transgenic wheat lines, the full-length coding sequence of TaHRP1 was introduced into the pEarleyGate 104 vector with YFP at the C-terminus using Gateway technology. The recombinant vector was transformed into *A. tumefaciens* strain EHA105, and the transformed strains were infiltrated into the immature embryos of the wheat cultivar Fielder. The total proteins of the positive transgenic seedlings were extracted and detected via western blotting using an anti-GFP antibody (Beyotime, cat.no. AG281, 1:2000).

Subcellular localization and BIFC assays

For subcellular localization in *N. benthamiana* leaves, the full-length coding sequences of *TaPIR1* and *TaHRP1* were cloned into the pCAMBIA1302 vector and transformed into *A. tumefaciens* GV3101. The transformed strains with the corresponding constructs were infiltrated into *N. benthamiana* leaves through *A. tumefaciens*-mediated infiltration at a final optical density at 600 nm (OD₆₀₀) of 0.6. For subcellular localization in wheat protoplasts, the full-length coding sequences of *TaPIR1* and *TaHRP1* were cloned into the pJIT163-GFP vector and then transfected into wheat protoplasts via PEG-mediated transfection⁶⁰. The GFP signal of protoplasts was observed using a confocal microscope. For the BIFC assay, *TaPIR1* and *TaHRP1* were ligated with YFP in pSPYNE and pSPYCE vectors, respectively, and these constructs were transformed into *A. tumefaciens* GV3101⁶¹. The *Agrobacterium* strains carrying BIFC and NLS-red fluorescent protein (RFP) recombinant

vectors were infiltrated into *N. benthamiana* leaves at an OD₆₀₀ of 0.5. Images were captured at 48 hpi via confocal microscopy using a 488 nm laser.

Yeast two-hybrid assays

The full-length coding sequence of *TaPIRI* was cloned into the pGBKT7 vector as bait to screen a cDNA library of pathogen-infected wheat. The bait construct and Y2H cDNA library plasmids were cotransformed into the yeast strain AH109, which was then inoculated into an SD/-His/-Leu/-Trp/-Ade medium to screen for potential *TaPIRI*-interacting proteins, according to the Matchmaker Y2H system protocol (CLONTECH Laboratories). Potentially interacting proteins were screened and introduced into the pGADT7 vector as prey proteins. The bait and different prey proteins were cotransfected into the yeast strain AH109, and the diluted yeast cells were then inoculated into an SD/-Ade/-His/-Leu/-Trp medium supplemented with X- α -Gal. Images were captured after 3-day incubation at 30 °C.

Split luciferase complementation assay

The split-luciferase complementation assay was performed as previously described⁶². The full-length coding sequences of *TaPIRI* and *TaHRP1* were cloned into JW771-NLuc and JW772-CLuc vectors, respectively, and then infiltrated into *N. benthamiana* leaves via *Agrobacterium*-mediated transformation. The infiltrated plants were cultured in a greenhouse for 48 h at 23 °C, and the infiltrated leaves were smeared with D-luciferin (Coolaber, cat.no. CL6928) and incubated for 10 min under dark conditions. Images were captured using a CCD imaging system (VILBER, France).

Coimmunoprecipitation assays

For the Co-IP assay, *A. tumefaciens* GV3101 carrying *TaHRP:HA* and *TaPIRI:GFP* was infiltrated into *N. benthamiana* leaves via *Agrobacterium*-mediated transformation. After 48 h of infiltration, the total proteins in the infiltrated leaves were extracted using NP-40 lysis buffer (Beyotime, cat.no. P0013F) with 1 mM phenylmethanesulfonyl fluoride (Beyotime, cat.no. ST506), 1% Protease inhibitor cocktail (Beyotime, cat.no. P1005) and 50 μ M MG132 (Selleck, cat.no. S2619). The extracted proteins were then incubated with GFP-trap agarose (ChromoTek, cat.no. gta-20) at 4 °C for 2 h, following the manufacturer's instructions. The agarose beads were collected via centrifugation at 2500 \times g and 4 °C for 5 min and washed three times with 500 μ L of phosphate buffer saline and 0.5% Tween-20. The proteins bound to GFP-trap agarose were boiled for 10 min and detected via western blotting with anti-GFP (Beyotime, cat.no. AG281, 1:2000) or anti-HA antibody (Beyotime, cat.no. AH158, 1:2000).

Nucleic and cytoplasmic extract preparation assay

TaHRP:GFP or *GFP* vectors were transiently expressed in *N. benthamiana* leaves via *Agrobacterium*-mediated transformation. The infiltrated leaves were ground to a fine powder using liquid nitrogen and then homogenized using Honda buffer (2.5% Dextran T40, 1.25% Ficoll 400, 10 mM MgCl₂, 0.44 M sucrose, 20 mM HEPES-KOH, pH 7.4, 5 mM DTT, 1 mM PMSF, 0.5% Triton X-100, and 1% protease inhibitor cocktail) as previously described⁶³. The extract was filtered through three layers of gauze into a 30-mL tube and then centrifuged at 3000 \times g and 4 °C for 10 min. The precipitates were washed three times with Honda buffer and centrifuged at 4000 \times g. For immunodetection, the supernatant sample and pellet resuspended in NP-40 lysis buffer were incubated with SDS loading buffer at 95 °C for 10 min.

In vitro pull-down assay

TaPIRI and *TaHRP1* fragments were cloned into pET32a and pGEX-6P-1 vectors to purify *TaPIRI:His* and *TaHRP1:GST* recombinant proteins, respectively. The tagged proteins were subjected to in vitro pull-down assay⁶⁴. For affinity purification, mixtures of equal amounts of

TaHRP1:GST and *TaPIRI:His*, as well as *GST* and *TaPIRI:His* were incubated at 4 °C for 1.5 h and mixed with glutathione resins. Recombinant protein mixtures and proteins eluted from glutathione resins were detected with anti-His (Beyotime, cat.no. AF5060, 1:2000) or anti-GST antibody (Beyotime, cat.no. AG768, 1:2000).

Ubiquitination assay

For in vivo ubiquitination assay, *TaPIRI:HA* or *TaPIR1M:HA* and *TaHRP1:GFP*, three mutated versions of *TaHRP1:GFP* (*TaHRP1*^{K131R}, *TaHRP1*^{K136R}, and *TaHRP1*^{K131/136R}) and *TaPIRI:HA* were transiently expressed in *N. benthamiana* leaves via *Agrobacterium*-mediated transformation⁶⁵. The infiltrated leaves were injected with 50 μ M MG132 for 10 h before extracting total proteins. For the in vivo ubiquitination assay in wheat protoplasts, *TaPIRI:HA* and *TaHRP1:GFP* were co-transfected into wheat protoplasts via PEG-mediated transfection and pretreated with MG132 for 12 h before protein extraction. Proteins were extracted and incubated with GFP-trap agarose for protein enrichment. The proteins bound to GFP-trap agarose were boiled for 10 min and detected via western blotting with anti-GFP and anti-ubiquitin antibodies (HUABIO, cat.no. ET1609-21, 1:1000).

The in vitro ubiquitination assay was conducted⁶⁶. The coding sequences of *TaPIRI* and *TaHRP1* were cloned into pET32a and pGEX-6P-1 vectors, respectively, and were purified from *E. coli* BL21 cells using standard protocols. Each reaction of the ubiquitination assay was performed in a 30- μ L mixture containing 0.3 μ g of E1 (R&D SYSTEMS, cat.no. E-305-025), 0.5 μ g of E2 (R&D SYSTEMS, cat.no. E2-622-100), 2 μ g of ubiquitin (R&D SYSTEMS, cat.no. U-530), 0.5 μ g of *TaPIRI:His*, and 0.5 μ g of *TaHRP1:GST*, mutated versions of *TaHRP1:GST* (*TaHRP1*^{K131R}, *TaHRP1*^{K136R}, and *TaHRP1*^{K131/136R}) or *GST*, and ubiquitination buffer (50 mM Tris-HCl, pH 7.4, 2 mM ATP, 5 mM MgCl₂, 2 mM DTT, 40 μ M ZnSO₄); this mixture was incubated at 30 °C for 3 h. For immunoblotting, the samples were incubated with an SDS loading buffer at 95 °C for 10 min. The ubiquitinated *TaHRP1:GST* proteins were detected with anti-ubiquitin and anti-GST antibodies, and the *TaPIRI:His* proteins were detected with anti-His antibodies.

Protein degradation assay

For the in vivo protein degradation assay, the *TaPIRI:GFP* and *TaPIRI:HA* recombinant vectors were transiently expressed in *N. benthamiana* leaves via *Agrobacterium*-mediated transformation. The infiltrated leaves were injected with 50 μ M MG132 for 10 h before extracting total proteins using NP-40 lysis buffer. The extracted proteins were then incubated with an SDS loading buffer at 95 °C for 10 min for immunoblotting. The *TaPIRI:GFP* and *TaPIRI:HA* proteins were detected with anti-GFP and anti-HA antibodies, respectively.

For the semi-in vivo protein degradation assay, one of the four recombinant proteins—*TaHRP1:GST*, *TaHRP1*^{K131R}:*GST*, *TaHRP1*^{K136R}:*GST*, *TaHRP1*^{K131/136R}:*GST*, or *GST*—was incubated with the total protein extracted from *Fielder*, *tapir1-AB*, and *TaPIRI*-overexpressing plants in an environment supplemented with 2 mM ATP and 50 μ M MG132 or DMSO at 28 °C for 0 min, 15 min, 30 min, and 60 min. *TaHRP1:GST* protein was detected via western blotting with an anti-GST antibody. Quantitative analysis of the immunoblots was performed using the quantity tools of ImageJ software.

DNA affinity purification and sequencing analysis

DAP-seq was performed at Bluescape Hebei Biotech following the method described in a previous study⁶⁷. Briefly, genomic DNA was extracted from *Fielder* plants and fragmented to an average length of 200 bp using Covaris M220 (Woburn, MA, USA)⁶⁸. A fragmented genomic DNA library was constructed using MICH TLX DNA-Seq Kit (Bluescape Hebei Biotech, cat.no. NGS0602). The full-length coding sequence of *TaHRP1* was introduced into the pFN19K HaloTag T7 SP6 Flexi expression vector and expressed in vitro using the TNT SP6-coupled wheat germ extract system (Promega). Expressed *TaHRP1*

proteins were directly captured using Magne Halo Tag Beads (Promega) and incubated with the genomic DNA library; the genes were subsequently sequenced using the Illumina NavoSeq sequencing platform at Bluescape Hebei Biotech. Peak calling of the two biological duplicates was merged using MACS2 callpeak and Homer software with a q -value of <0.05 , and conservative motifs were analyzed using MEME-CHIP software.

EMSA

The EMSA was performed using Light Shift Chemiluminescent EMSA Kit (Thermo Fisher Scientific, cat.no. 20158) following the manufacturer's instructions. The promoter fragment of TaPetN containing an HBS element with a 60-bp flanking sequence upstream and downstream was biotinylated and synthesized by Sangon Biotech (Shanghai, China). The recombinant protein TaHRP1:GST, TaHRP^{HA}:GST, or GST at the corresponding concentration was incubated with each probe in 5× EMSA/Gel-Shift binding buffer for 30 min at room temperature. To determine the binding specificity, unlabeled or mutated biotin-labeled probes were added to the reaction mixture as the mProbe control. The products were then separated via 6% native polyacrylamide gel electrophoresis under 80 V for 1.5 h in 0.5× TBE buffer and transferred onto a positively charged nylon membrane (Millipore, cat.no. INYC00010). The binding bands on the membrane were detected using a chemiluminescent nucleic acid module. Supplementary Data 2 lists the probe sequences used in EMSA.

Transient dual-luciferase reporter assay

To evaluate the transcriptional activity of TaHRP1, promoter fragments of PhANGs containing an HBS element with a 1000-bp flanking sequence upstream and downstream were cloned into the pGreen II 0800-LUC vector, and the coding sequence of TaHRP1 was cloned into the pGreen II 62SK vector⁶⁹. Supplementary Data 2 presents the primers used in this experiment. The corresponding reporter and effector constructs were simultaneously transformed into *N. benthamiana* leaves. After 48 h of infiltration, firefly luciferase (LUC) and Renilla luciferase (REN) activities were detected using Dual-Luciferase Reporter Assay Kit (Vazyme, cat.no. DL101) following the manufacturer's instructions.

Detection of chlorophyll fluorescence

The chlorophyll fluorescence parameters were measured using the MINI-PAM system (Walz, Effeltrich, Germany) following the manufacturer's instructions and a previously described protocol⁵². Four-week-old *N. benthamiana* plants were infiltrated with *Agrobacterium* harboring the indicated vectors and cultured under conditions of 8-h/16-h light/dark. To quantify Fv/Fm, the leaves were dark-adapted using the manufacturer's leaf clips for 30 min at room temperature and then exposed to a saturating light pulse ($5000 \mu\text{mol m}^{-2} \text{s}^{-1}$ for 0.8 s). Minimal fluorescence (F_0) and maximal fluorescence F_m were monitored with a very weak light ($0.04 \mu\text{mol m}^{-2} \text{s}^{-1}$) and a transient saturated light pulse ($5000 \mu\text{mol m}^{-2} \text{s}^{-1}$). Maximum quantum yield (Fv/Fm) was calculated as $(F_m - F_0)/F_m$. Actinic light ($120 \mu\text{mol m}^{-2} \text{s}^{-1}$ —the same as plant growth light intensity) was then applied for 15 min, followed by a saturating pulse to obtain maximal fluorescence (F_m'), and minimal fluorescence F_0' after turning off the actinic light was measured. NPQ was calculated as $1 - (F_m' - F_0')/(F_m - F_0)$. Photoirradiance response curves (LRC) were measured using different actinic light intensities ($25 \mu\text{mol m}^{-2} \text{s}^{-1}$, $45 \mu\text{mol m}^{-2} \text{s}^{-1}$, $65 \mu\text{mol m}^{-2} \text{s}^{-1}$, $90 \mu\text{mol m}^{-2} \text{s}^{-1}$, $125 \mu\text{mol m}^{-2} \text{s}^{-1}$, $190 \mu\text{mol m}^{-2} \text{s}^{-1}$, $285 \mu\text{mol m}^{-2} \text{s}^{-1}$, $420 \mu\text{mol m}^{-2} \text{s}^{-1}$, $625 \mu\text{mol m}^{-2} \text{s}^{-1}$, $820 \mu\text{mol m}^{-2} \text{s}^{-1}$, $1150 \mu\text{mol m}^{-2} \text{s}^{-1}$, and $1500 \mu\text{mol m}^{-2} \text{s}^{-1}$), and each lasted for 30 s in the dark. LRC is a function of the ETR in response to PAR as shown in the following equation: $\text{ETR} = \text{PAR} \times \text{ETR factor} \times (\text{PPS}_2/\text{PPS}_{1+2}) \times Y(\text{II})$, where PAR is photosynthetic active radiation, and ETR factor and $(\text{PPS}_2/\text{PPS}_{1+2})$ are constants with values of 0.84 and 0.5, respectively. Light intensity was

monitored using WinControl 2.3 software. Measurement of 6–8 leaves was performed per replicate, and three biological replicates were examined.

BSMV-mediated gene silencing and gene overexpression

For transient silencing of *TaPIR1*, a specific fragment of *TaPIR1* was inserted into the BSMV construct. Each BSMV construct was linearized and transcribed to RNA and then inoculated into the second leaves⁷⁰. For *TaPIR1* expression in wheat leaves, the full-length genes were inserted into the BSMV-VOX vector. The vector containing the tripartite viral genome and recombinant vectors was linearized and transcribed into RNA in vivo. Transcripts of each construct were mixed in a 1:1:1 ratio and then added to 200 μL of FES buffer. Seedlings treated with the virus were grown at 25–27 °C. After 10 days, the fourth leaves were inoculated with *Pst* urediniospores. The *Pst*-infected leaves were sampled at 24 hpi and 48 hpi for silencing efficiency assessment and at 120 hpi for fungal biomass assay. Leaves infected with *Pst* urediniospores were observed at 14 dpi.

Histochemical assay

To observe fungal hyphae, the infected leaf tissues were cleaned with ethanol and autoclaved using 1 M KOH at 121 °C for 5–6 min. Leaf fragments were carefully washed three times with 2 mL of 50 mM Tris-HCl (pH 7.4) and incubated in wheat germ agglutinin solution (Alexa-488; Thermo Fisher Scientific)⁷¹. Hyphal length and infection areas were observed using an Olympus BX-51 microscope.

For the H_2O_2 detection assay, the infected leaf tissues were incubated in 1.0 mg/mL DAB solution under light conditions for 4 h at 16 °C. Subsequently, the samples were treated with ethanol, as mentioned above, to remove chlorophyll, and H_2O_2 was observed and measured as a reddish-brown color under microscopy using the CellSens Entry program⁷². We also used the probe 2',7'-dichlorodihydrofluorescein diacetate ($\text{H}_2\text{DCF-DA}$) to observe ROS accumulation in chloroplasts⁷³. Briefly, PhANGs were transiently expressed in tobacco and harvested at 36 hpi. A solution of 10 μM $\text{H}_2\text{DCF-DA}$ in 10 mM MgCl_2 buffer was injected into the infiltrated leaves using a syringe. For H_2O_2 detection in wheat protoplasts, TaHRP1, TaHRP1^{HA}, and *TaPIR1* were transfected into wheat protoplasts via PEG-mediated transfection, following which the wheat protoplasts were harvested at 36 hpi and treated with 10 μM $\text{H}_2\text{DCF-DA}$ in 10 mM MgCl_2 buffer. Chloroplast-derived ROS were visualized and imaged via confocal microscopy under laser excitation at 488 nm and emission at 530 nm.

Genomic DNA and RNA extraction and qRT-PCR analysis

Genomic DNA was extracted from the second leaves of two-leaf stage Fielder and transgenic plants using the CTAB method⁷⁴. DNA from *Pst*-infected leaves was extracted at 5 dpi for fungal biomass analysis. *Pst* biomass was calculated using the cycle threshold (Ct) value of *PstEF* DNA against the Ct of wheat genomic elongation factor DNA (*TaEFI*). Total RNA was extracted from *Pst*-infected wheat leaves using MiniBEST Plant RNA Extraction Kit (Takara, Dalian, China) following the manufacturer's instructions. First-strand cDNA synthesis was performed using the GoScript reverse transcription system (Promega Corp.). *TaEF* and *PstEF* were used to normalize the RNA levels of wheat leaves and *Pst*, respectively. Data from three independent biological replicates were analyzed using Student's t -test.

Statistics and reproducibility

Image Lab (version 4.0) build 16 was used for DNA electrophoresis and WB data collection. The micrographs were collected by Leica LAS X Hardware Configurator Version 2020.6.0. MEME Suite 5.4.1 was used for analyzing conserved motifs. The sequence alignment was performed using <http://multalin.toulouse.inra.fr/multalin/multalin.html>. MEME Suite 5.4.1 was used for analyzing conserved motifs. All data

analysis was performed using GraphPad 8.0 and is shown as means \pm standard deviation (SD). The statistical analyses were performed using SPSS 26.0. The significant differences between experimental and control groups were determined by the two-tailed Student's *t*-test, and one-way ANOVA. Analytical methods, *n*-values, and *P* values can be found in the figures or figure legends. All experiments in this study were performed two to and multiple times with similar results. No data were excluded from the analyses. The investigators were not blinded to allocation during experiments and outcome assessment.

Reporting summary

Further information on research design is available in the Nature Portfolio Reporting Summary linked to this article.

Data availability

GenBank accession codes include XP_037425335 for *TaP1R1* genes and XP_044353823 for *TaHRP1* genes (<https://www.ncbi.nlm.nih.gov/>). DAP-seq data in this study has been uploaded to the NCBI Sequence Read Archive under the accessions PRJNA1066020. All data supporting the findings of this work are available in the paper, Supplementary Information files, and repository platform. Source data are provided with this paper.

References

- Jones, J. D. & Dangl, J. L. The plant immune system. *Nature* **444**, 323–329 (2006).
- Ngou, B. P. M., Ding, P. & Jones, J. D. G. Thirty years of resistance: zig-zag through the plant immune system. *Plant cell* **34**, 1447–1478 (2022).
- Dodds, P. N. & Rathjen, J. P. Plant immunity: towards an integrated view of plant-pathogen interactions. *Nat. Rev. Genet.* **11**, 539–548 (2010).
- Chinchilla, D. et al. A flagellin-induced complex of the receptor FLS2 and BAK1 initiates plant defence. *Nature* **448**, 497–500 (2007).
- Boller, T. & He, S. Y. Innate immunity in plants: an arms race between pattern recognition receptors in plants and effectors in microbial pathogens. *Science* **324**, 742–744 (2009).
- Iwasaki, A. & Medzhitov, R. Regulation of adaptive immunity by the innate immune system. *Science* **327**, 291–295 (2010).
- Zipfel, C. & Oldroyd, G. E. D. Plant signalling in symbiosis and immunity. *Nature* **543**, 328–336 (2017).
- Rekhter, D. et al. Isochorismate-derived biosynthesis of the plant stress hormone salicylic acid. *Science* **365**, 498–502 (2019).
- Torrens-Spence, M. P. et al. PBS3 and EPS1 complete salicylic acid biosynthesis from isochorismate in *Arabidopsis*. *Mol. plant* **12**, 1577–1586 (2019).
- Nomura, H. et al. Chloroplast-mediated activation of plant immune signalling in *Arabidopsis*. *Nat. Commun.* **3**, 926 (2012).
- Pfannschmidt, T. Chloroplast redox signals: how photosynthesis controls its own genes. *Trends Plant Sci.* **8**, 33–41 (2003).
- Serrano, I., Audran, C. & Rivas, S. Chloroplasts at work during plant innate immunity. *J. Exp. Bot.* **67**, 3845–3854 (2016).
- Lv, R. et al. Uncoupled expression of nuclear and plastid photosynthesis-associated genes contributes to cell death in a lesion mimic mutant. *Plant cell* **31**, 210–230 (2019).
- Li, M. & Kim, C. CHAPTER one—singlet oxygen in plants: from genesis to signaling. In *Advances in Botanical Research* (eds. Mittler, R. O. N. & Breusegem, F. V.) (Academic Press, 2023).
- Li, X.-P., Müller-Moulé, P., Gilmore, A. M. & Niyogi, K. K. PsbS-dependent enhancement of feedback de-excitation protects photosystem II from photoinhibition. *Proc. Natl. Acad. Sci.* **99**, 15222–15227 (2002).
- Wang, S. et al. YR36/WKS1-mediated phosphorylation of PsbO, an extrinsic member of photosystem II, inhibits photosynthesis and confers stripe rust resistance in wheat. *Mol. plant* **12**, 1639–1650 (2019).
- Wang, X. et al. Two stripe rust effectors impair wheat resistance by suppressing import of host Fe-S protein into chloroplasts. *Plant Physiol.* **187**, 2530–2543 (2021).
- French, M. E., Koehler, C. F. & Hunter, T. Emerging functions of branched ubiquitin chains. *Cell Discov.* **7**, 6 (2021).
- Swatek, K. N. & Komander, D. Ubiquitin modifications. *Cell Res.* **26**, 399–422 (2016).
- Stone, S. L. et al. Functional analysis of the RING-type ubiquitin ligase family of *Arabidopsis*. *Plant Physiol.* **137**, 13–30 (2005).
- Vierstra, R. D. The ubiquitin–26S proteasome system at the nexus of plant biology. *Nat. Rev. Mol. Cell Biol.* **10**, 385–397 (2009).
- Fu, S. et al. An evolutionarily conserved C4HC3-type E3 ligase regulates plant broad-spectrum resistance against pathogens. *Plant cell* **34**, 1822–1843 (2022).
- Gao, M. et al. Ca²⁺ sensor-mediated ROS scavenging suppresses rice immunity and is exploited by a fungal effector. *Cell* **184**, 5391–5404.e5317 (2021).
- Wang, R., Xu, X., Wang, G.-L. & Ning, Y. Ubiquitination of susceptibility proteins modulates rice broad-spectrum resistance. *Trends Plant Sci.* **27**, 322–324 (2022).
- Liu, Q. et al. OsCUL3a negatively regulates cell death and immunity by degrading OsNPR1 in rice. *Plant Cell* **29**, 345–359 (2017).
- Wang, Y. et al. Transcriptome analysis provides insights into the mechanisms underlying wheat cultivar Shumai26 responding to stripe rust. *Gene* **768**, 145290 (2021).
- Gaudet, P., Livstone, M. S., Lewis, S. E. & Thomas, P. D. Phylogenetic-based propagation of functional annotations within the gene ontology consortium. *Brief Bioinform.* **12**, 449–462 (2011).
- Kachroo, P., Burch-Smith, T. M. & Grant, M. An emerging role for chloroplasts in disease and defense. *Annu. Rev. Phytopathol.* **59**, 423–445 (2021).
- Ning, Y. et al. OsELF3-2, an ortholog of *Arabidopsis* ELF3, interacts with the E3 ligase APIP6 and negatively regulates immunity against *Magnaporthe oryzae* in rice. *Mol. plant* **8**, 1679–1682 (2015).
- Park, C.-H. et al. The *Magnaporthe oryzae* effector AvrPiz-t targets the RING E3 ubiquitin ligase APIP6 to suppress pathogen-associated molecular pattern-triggered immunity in rice. *Plant cell* **24**, 4748–4762 (2012).
- Langner, T., Kamoun, S. & Belhaj, K. CRISPR crops: plant genome editing toward disease resistance. *Annu. Rev. Phytopathol.* **56**, 479–512 (2018).
- Zaidi, S. S., Mukhtar, M. S. & Mansoor, S. Genome editing: targeting susceptibility genes for plant disease resistance. *Trends Biotechnol.* **36**, 898–906 (2018).
- Li, S. et al. Genome-edited powdery mildew resistance in wheat without growth penalties. *Nature* **602**, 455–460 (2022).
- Wang, N. et al. Inactivation of a wheat protein kinase gene confers broad-spectrum resistance to rust fungi. *Cell* **185**, 2961–2974.e2919 (2022).
- Wang, N. et al. Transcriptional repression of TaNOX10 by TaWRKY19 compromises ROS generation and enhances wheat susceptibility to stripe rust. *Plant Cell* **34**, 1784–1803 (2022).
- Hara, M., Fujinaga, M. & Kuboi, T. Metal binding by citrus dehydrin with histidine-rich domains. *J. Exp. Bot.* **56**, 2695–2703 (2005).
- Hara, M., Shinoda, Y., Tanaka, Y. & Kuboi, T. DNA binding of citrus dehydrin promoted by zinc ion. *Plant, Cell Environ.* **32**, 532–541 (2009).
- Hernández-Sánchez, I. et al. Nuclear localization of the dehydrin OpsDHN1 is determined by histidine-rich motif. *Front. plant Sci.* **6**, 702 (2015).
- Göhre, V. Immune responses: photosynthetic defence. *Nat. Plants* **1**, 15079 (2015).

40. Breen, S. et al. Chloroplasts play a central role in facilitating MAMP-triggered immunity, pathogen suppression of immunity and crosstalk with abiotic stress. *Plant Cell Environ.* **45**, 3001–3017 (2022).
41. Kim, S. H. et al. The *Arabidopsis* immune adaptor SRRF1 interacts with TCP transcription factors that redundantly contribute to effector-triggered immunity. *Plant J.* **78**, 978–989 (2014).
42. Weßling, R. et al. Convergent targeting of a common host protein network by pathogen effectors from three kingdoms of life. *Cell Host Microbe* **16**, 364–375 (2014).
43. Schwenkert, S. et al. Role of the low-molecular-weight subunits PetL, PetG, and PetN in assembly, stability, and dimerization of the cytochrome b6f complex in tobacco. *Plant Physiol.* **144**, 1924–1935 (2007).
44. Alazem, M., Tseng, K.-C., Chang, W.-C., Seo, J.-K. & Kim, K.-H. Elements involved in the Rsv3-mediated extreme resistance against an avirulent strain of soybean mosaic virus. *Viruses* **10**, 581 (2018).
45. Ruuska, S. A., Andrews, T. J., Badger, M. R., Price, G. D. & von Caemmerer, S. The role of chloroplast electron transport and metabolites in modulating rubisco activity in tobacco. Insights from transgenic plants with reduced amounts of cytochrome b/f complex or glyceraldehyde 3-phosphate dehydrogenase1. *Plant Physiol.* **122**, 491–504 (2000).
46. Yamori, W. et al. The roles of ATP synthase and the cytochrome b6/f complexes in limiting chloroplast electron transport and determining photosynthetic capacity. *Plant Physiol.* **155**, 956–962 (2010).
47. Bwalya, J., Alazem, M. & Kim, K.-H. Photosynthesis-related genes induce resistance against soybean mosaic virus: Evidence for involvement of the RNA silencing pathway. *Mol. Plant Pathol.* **23**, 543–560 (2022).
48. Bilgin, D. D. et al. Biotic stress globally downregulates photosynthesis genes. *Plant Cell Environ.* **33**, 1597–1613 (2010).
49. Bhattacharyya, D. & Chakraborty, S. Chloroplast: the trojan horse in plant–virus interaction. *Mol. plant Pathol.* **19**, 504–518 (2018).
50. Kretschmer, M., Croll, D. & Kronstad, J. W. Chloroplast-associated metabolic functions influence the susceptibility of maize to *Ustilago maydis*. *Mol. Plant Pathol.* **18**, 1210–1221 (2017).
51. Xu, Q. et al. An effector protein of the wheat stripe rust fungus targets chloroplasts and suppresses chloroplast function. *Nat. Commun.* **10**, 5571 (2019).
52. de Torres Zabala, M. et al. Chloroplasts play a central role in plant defence and are targeted by pathogen effectors. *Nat. Plants* **1**, 15074 (2015).
53. Rodríguez-Herva, J. J. et al. A bacterial cysteine protease effector protein interferes with photosynthesis to suppress plant innate immune responses. *Cell. Microbiol.* **14**, 669–681 (2012).
54. Kuźniak, E. & Kopczeński, T. The chloroplast reactive oxygen species-redox system in plant immunity and disease. *Front. Plant Sci.* **11**, 572686 (2020).
55. Oukarroum, A., Bussotti, F., Goltsev, V. & Kalaji, H. M. Correlation between reactive oxygen species production and photochemistry of photosystems I and II in *Lemna gibba* L. plants under salt stress. *Environ. Exp. Bot.* **109**, 80–88 (2015).
56. Moustakas, M., Moustaka, J. & Sperdoui, I. Hormesis in photosystem II: a mechanistic understanding. *Curr. Opin. Toxicol.* **29**, 57–64 (2022).
57. Kang, Z., Huang, L. & Buchenauer, H. Ultrastructural changes and localization of lignin and callose in compatible and incompatible interactions between wheat and *Puccinia striiformis*. *Z. Pflanzenschutz. Pflanzenschutz* **109**, 25–37 (2002).
58. Ma, S. et al. WheatOmics: a platform combining multiple omics data to accelerate functional genomics studies in wheat. *Mol. Plant* **14**, 1965–1968 (2021).
59. Zhang, Z. et al. Development of an *Agrobacterium*-delivered CRISPR/Cas9 system for wheat genome editing. *Plant Biotechnol. J.* **17**, 1623–1635 (2019).
60. Yoo, S.-D., Cho, Y.-H. & Sheen, J. *Arabidopsis* mesophyll protoplasts: a versatile cell system for transient gene expression analysis. *Nat. Protoc.* **2**, 1565–1572 (2007).
61. Waadt, R. et al. Multicolor bimolecular fluorescence complementation reveals simultaneous formation of alternative CBL/CIPK complexes in planta. *Plant J.* **56**, 505–516 (2008).
62. Wang, L., Yu, G., Macho, A. P. & Lozano-Durán, R. Split-luciferase complementation imaging assay to study protein-protein interactions in *Nicotiana benthamiana*. *Bio Protoc.* **11**, e4237 (2021).
63. Xing, D., Wang, Y., Hamilton, M., Ben-Hur, A. & Reddy, A. S. N. Transcriptome-wide identification of RNA targets of *Arabidopsis* SERINE/ARGININE-RICH45 uncovers the unexpected roles of this RNA binding protein in RNA processing. *Plant Cell* **27**, 3294–3308 (2015).
64. Swaffield, J. C. & Johnston, S. A. Affinity purification of proteins binding to GST fusion proteins. *Curr. Protoc. Mol. Biol.* **33**, 20.22.21–20.22.10 (1996).
65. Liu, L. et al. An efficient system to detect protein ubiquitination by agroinfiltration in *Nicotiana benthamiana*. *Plant J.* **61**, 893–903 (2010).
66. Xie, Q. et al. SINAT5 promotes ubiquitin-related degradation of NAC1 to attenuate auxin signals. *Nature* **419**, 167–170 (2002).
67. Galli, M. et al. The DNA binding landscape of the maize AUXIN RESPONSE FACTOR family. *Nat. Commun.* **9**, 4526 (2018).
68. Zhang, Y. et al. Transposable elements orchestrate subgenome-convergent and divergent transcription in common wheat. *Nat. Commun.* **13**, 6940 (2022).
69. Guo, X. et al. The PGS1 basic helix–loop–helix protein regulates FL3 to impact seed growth and grain yield in cereals. *Plant Biotechnol. J.* **20**, 1311–1326 (2022).
70. Holzberg, S., Brosio, P., Gross, C. S. & Pogue, G. P. Barley stripe mosaic virus-induced gene silencing in a monocot plant. *Plant J.* **30**, 315–327 (2002).
71. Xu, Q. et al. Haustoria – arsenals during the interaction between wheat and *Puccinia striiformis* f. sp. *tritici*. *Mol. plant Pathol.* **21**, 83–94 (2020).
72. Li, Y. et al. TaRBP1 stabilizes TaGLTP and negatively regulates stripe rust resistance in wheat. *Mol. plant Pathol.* **24**, 1205–1219 (2023).
73. Zurbriggen, M. D. et al. Chloroplast-generated reactive oxygen species play a major role in localized cell death during the non-host interaction between tobacco and *Xanthomonas campestris* pv. *vesicatoria*. *Plant J.* **60**, 962–973 (2010).
74. Healey, A., Furtado, A., Cooper, T. & Henry, R. J. Protocol: a simple method for extracting next-generation sequencing quality genomic DNA from recalcitrant plant species. *Plant Methods* **10**, 1–8 (2014).

Acknowledgements

We thank Prof. Qixin Sun and Mingming Xin (China Agricultural University) for providing the pBUE411 vector used in this study. This study was supported by the National Natural Science Foundation of China (32102229) to Q.X., the Biotech Breeding Program of State Key Laboratory of Crop Gene Exploration and Utilization in Southwest China (SKL-ZY202233) to Q.X., the Sichuan Science and Program (2024NSFC0405 and 2021YJ0298) to Q.X., and the Sichuan Science and Technology Program, China (2022ZDZX0014) to Y. Wei.

Author contributions

Q.X., R.Z., and Y. Wei designed the research. R.Z., Y. Wu, and W.Y. conducted most of the experiments. X.Q. constructed vectors and performed the photosynthesis assay and BIFC assay. Q.W. and Y. Wu cultured tobacco and wheat plants. L.H., J.M., Y.Z., G.C., P.Q., Y.J., Q.J.

and Y.Z. provided technical support. R.Z., X.W., Y. Wei, and Q.X. wrote and revised this manuscript.

Competing interests

The authors declare no competing interests.

Additional information

Supplementary information The online version contains supplementary material available at <https://doi.org/10.1038/s41467-024-51249-1>.

Correspondence and requests for materials should be addressed to Xiaojie Wang, Yuming Wei or Qiang Xu.

Peer review information *Nature Communications* thanks Zhiyong Liu, and the other, anonymous, reviewer(s) for their contribution to the peer review of this work. A peer review file is available.

Reprints and permissions information is available at <http://www.nature.com/reprints>

Publisher's note Springer Nature remains neutral with regard to jurisdictional claims in published maps and institutional affiliations.

Open Access This article is licensed under a Creative Commons Attribution-NonCommercial-NoDerivatives 4.0 International License, which permits any non-commercial use, sharing, distribution and reproduction in any medium or format, as long as you give appropriate credit to the original author(s) and the source, provide a link to the Creative Commons licence, and indicate if you modified the licensed material. You do not have permission under this licence to share adapted material derived from this article or parts of it. The images or other third party material in this article are included in the article's Creative Commons licence, unless indicated otherwise in a credit line to the material. If material is not included in the article's Creative Commons licence and your intended use is not permitted by statutory regulation or exceeds the permitted use, you will need to obtain permission directly from the copyright holder. To view a copy of this licence, visit <http://creativecommons.org/licenses/by-nc-nd/4.0/>.

© The Author(s) 2024, corrected publication 2025